Mediterranean Production Centre
MEDSEA_HINDCAST_WAV_006_012

Issue: 1.2

Contributors: Anna Zacharioudaki, Michalis Ravdas, Gerasimos Korres, Vladyslav Lyubartsev (Validator)

Approval date by the CMEMS product quality coordination team: 29/05/19

CHANGE RECORD

When the quality of the products changes, the QuID is updated and a row is added to this table. The third column specifies which sections or sub-sections have been updated. The fourth column should mention the version of the product to which the change applies.

Issue	Date	§	Description of Change	Author	Validated By
1.0	September 2017	All	Creation of the document	Anna Zacharioudaki	Emanuela Clementi (PQ Responsible)
1.1	January 2018		Extent of the multi-year product (MYP) by one year	Anna Zacharioudaki	Emanuela Clementi (PQ Responsible)
1.2	January 2019		Extent of the multi-year product (MYP) by one year	Anna Zacharioudaki	Vladyslav Lyubartsev (PQ Responsible)

Table of contents

I EXECUTIVE SUMMARY

I.1 Products covered by this document

This document describes the quality of the multi-year product (MYP) of the wave component of the Mediterranean Sea: MEDSEA_HINDCAST_WAV_006_012. This is a 12-year wave hindcast for the Mediterranean Sea covering the period February 2006 - December 2017.

The product includes 2D hourly instantaneous fields of: spectral significant wave height (Hm0), spectral moments (-1,0) wave period (Tm-10), spectral moments (0,2) wave period (Tm02), wave period at spectral peak / peak period (Tp), mean wave direction from (Mdir), wave principal direction at spectral peak, stokes drift U, stokes drift V, spectral significant wind wave height, spectral moments (0,1) wind wave period, mean wind wave direction from, spectral significant primary swell wave height, spectral moments (0,1) primary swell wave period, mean primary swell wave direction from, spectral significant secondary swell wave height, spectral moments (0,1) secondary swell wave period, mean secondary swell wave direction from.

Output data are produced at 1/24º horizontal resolution.

I.2 Summary of the results

The quality of the Med-MFC 12-year wave hindcast (2006-2017, Q1/2019) is assessed by comparison with in-situ and satellite observations. Hindcast-long qualification statistics are obtained for the base period 2006-2015 covered by the first version of the Med-MFC waves MYP (Q3/2017). Additional years are assessed through the computation of yearly statistics over the entire hindcast period.

The main results of the MEDSEA_HINDCAST_WAV_006_012 product quality assessment are summarized below:

Spectral Significant Wave Height (Hm0): Overall, the significant wave height is accurately simulated by the model. Considering the Mediterranean Sea as a whole, the typical difference with in-situ and satellite observations (RMSD) is 0.23 m and 0.27 m respectively whilst the bias is -0.01 m (2%) and -0.1 m (8%) respectively. In general, the model somewhat underestimates the observations for wave heights below 2-3 m whilst it somewhat overestimates the observations for higher waves. Its performance is better in winter when the wave conditions are well-defined. Spatially, the model performs optimally at offshore wave buoy locations and well-exposed Mediterranean sub-regions. Within enclosed basins and near the coast, unresolved topography by the wind and wave models and fetch limitations cause the wave model performance to deteriorate.

Spectral moments (0,2) wave period (Tm02): The mean wave period is reasonably well simulated by the model. The typical difference with observations (RMSD) is 0.69 s and is mainly caused by model bias which has a value of -0.44 s (11%). Overall, the model underestimates wave periods below 6 s and overestimates larger periods. It also exhibits greater variability than the observations. Model performance is a little better in winter when wave conditions are well-defined. Spatially, the model mostly overestimates the highest mean wave period values in the western Mediterranean Sea, west and south of France. Otherwise, model underestimate is widespread at most of the locations

examined. Similarly to the wave height, the model performance is best at well-exposed offshore locations and deteriorates, mainly due to fetch limitations, at locations that are near the shore and/or are surrounded by complex topography.

Other variables: No observations are available for all other variables except for the wave period at spectral peak / peak period (Tp) and the mean wave direction from (Mdir). In contrast to Tm02 variation, which is smooth in the Mediterranean Sea, Tp variation is particularly spiky. As a result, validation of the latter wave parameter is thought to be less reliable and has not been considered herein despite data availability. On the other hand, qualification of Mdir will be considered in the near future. Generally, wave height variables are expected to be of similar quality to Hm0 and wave period variables to Tm02. Stokes drift quality is expected to be a function of both Hm0 and Tm02.

I.3 Estimated Accuracy Numbers

Estimated Accuracy Numbers (EANs), that are the mean and the RMS of the differences (RMSD) between the model and in-situ or satellite reference observations, are provided in Table 1 and Table 2 below. In following sections, "Mean" and "RMS" are referred to as "BIAS" and "RMSD" in alignment with metrics' name conventions within CMEMS.

EANs are computed for:

- Significant Wave Height (SWH): refers to the "spectral significant wave height (Hm0)"
- Mean Wave Period (MWP): refers to the "spectral moments (0,2) wave period (Tm02)"

The observations used are:

- in-situ observations from moored wave buoys obtained from the CMEMS INSITU_MED_NRT_OBSERVATIONS_013_035 dataset, available through the CMEMS In Situ Thematic Assemble Centre (INS-TAC)
- in-situ observations from moored Italian wave buoys obtained from ISPRA, Italy
- satellite altimeter observations from a merged altimeter wave height database setup at CERSAT - IFREMER (Queffeulou and Croizé-Fillon, 2017)

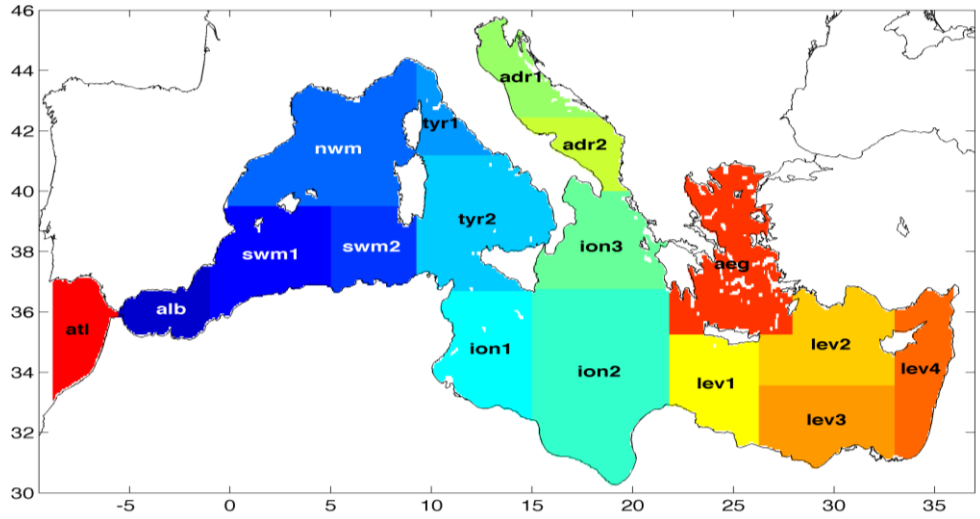

Figure 1: Mediterranean Sea sub-regions for validation metrics

The EANs computed for the CMEMS Mediterranean Sea multi-year wave system are based on a 12-year hindcast simulation from February 2006 to December 2017. They are provided as averages and standard deviations of yearly metric values. They are computed for the Mediterranean Sea as a whole and for 17 sub-regions from which 1 is in the Atlantic Ocean and 16 in the Mediterranean Sea (Figure 1): (atl) Atlantic, (alb) Alboran Sea, (swm1) West South-West Med, (swm2) East South-West Med, (nwm) North West Med, (tyr1) North Tyrrhenian Sea, (tyr2) South Tyrrhenian Sea, (adr1) North Adriatic Sea, (adr2) South Adriatic Sea, (ion1) South-West Ionian Sea, (ion2) South-East Ionian Sea, (ion3) North Ionian 3, (aeg) Aegean Sea, (lev1) West Levantine, (lev2) North-Central Levantine, (lev3) South-Central Levantine, (lev4) East Levantine. In particular, EANs based on comparisons between model and in-situ observations are calculated for the period 2007-2017 (2006 is incomplete and is excluded) corresponding to the current version of the MYP (Q1/2019). EANs based on comparisons between model and satellite observations are computed for the period 2007-2016 (inadequate observations were available to assess year 2017 because the CERCAT-IFREMER dataset reaches April 2017 while CMEMS altimeter SWH observations are not available before July 2017) which corresponds to the previous version of the MYP (Q2/2018).

SWH and MWP vs in-situ observations: full MED	Mean	RMS
SWH	-0.013 ± 0.014 m	0.231 ± 0.022 m
MWP	-0.44 ± 0.07 s	0.695 ± 0.035 s

Table 1: EANs of SWH and MWP evaluated for the current multi-year product (2006-2017): Averages and standard deviations of SWH-H-CLASS2-MOOR-BIAS-YR-MED, SWH-H-CLASS2-MOOR-RMSD-YR-MED, MWP-H-CLASS2-MOOR-BIAS-YR-MED, MWP-H-CLASS2-MOOR-RMSD-YR-MED in **Erreur ! Source du renvoi introuvable.**, Section III.

SWH vs satellite observations: full MED and sub-regions	Mean (m)	RMS (m)
MED	-0.102 ± 0.021	0.268 ± 0.020
atl	0.031 ± 0.034	0.262 ± 0.034
alb	-0.010 ± 0.025	0.278 ± 0.028
swm1	-0.084 ± 0.028	0.270 ± 0.026
swm2	-0.094 ± 0.027	0.291 ± 0.023
nwm	-0.096 ± 0.029	0.296 ± 0.027
tyr1	-0.127 ± 0.040	0.284 ± 0.035
tyr2	-0.109 ± 0.040	0.273 ± 0.031
ion1	-0.067 ± 0.017	0.232 ± 0.011
ion2	-0.091 ± 0.026	0.240 ± 0.024
ion3	-0.149 ± 0.044	0.295 ± 0.032
adr1	-0.180 ± 0.049	0.319 ± 0.030
adr2	-0.198 ± 0.054	0.317 ± 0.040
lev1	-0.093 ± 0.020	0.249 ± 0.022
lev2	-0.107 ± 0.026	0.241 ± 0.030
lev3	-0.109 ± 0.022	0.223 ± 0.025
lev4	-0.119 ± 0.020	0.238 ± 0.025
aeg	-0.068 ± 0.043	0.290 ± 0.034

Table 2: EANs of SWH evaluated for the 2006-2016 multi-year wave product (previous version) for the full Mediterranean Sea and the different sub-regions shown in Figure 1: Averages and standard deviations based on SWH-CLASS4-ALT-BIAS-YR-MED, SWH-CLASS4-ALT-RMSD-YR-MED, SWH-CLASS4-ALT-BIAS-YR-<REGION>, SWH-CLASS4-ALT-RMSD-YR-<REGION> in **Erreur ! Source du renvoi introuvable.**, Section III.

II PRODUCTION SYSTEM DESCRIPTION

II.1 Production centre details

Production Centre: Med-MFC

Production Unit: HCMR, Greece

Production System: Med-MFC multi-year wave hindcast

External product (2D): spectral significant wave height (Hm0), spectral moments (-1,0) wave period (Tm-10), spectral moments (0,2) wave period (Tm02), wave period at spectral peak / peak period (Tp), mean wave direction from (Mdir), wave principal direction at spectral peak, stokes drift U, stokes drift V, spectral significant wind wave height, spectral moments (0,1) wind wave period, mean wind wave direction from, spectral significant primary swell wave height, spectral moments (0,1) primary swell wave period, mean primary swell wave direction from, spectral significant secondary swell wave height, spectral moments (0,1) secondary swell wave period, mean secondary swell wave direction from.

Frequency of model output: hourly (instantaneous)

Geographical coverage: 18.125ºW → 36.2917ºE ; 30.1875ºN → 45.9792ºN

Horizontal resolution: 1/24º

Vertical coverage: Surface

Length of multi-year product: 12 years (Feb 2006 - Dec 2017)

Frequency of multi-year product release: Yearly (every year the multi-year product is extended by one year)

Reanalyses: No

Hindcast: Yes

II.2 Description of the Med-MFC wave hindcast modelling system

The multi-year wave product of the Mediterranean Monitoring and Forecasting Centre (Med-MFC) is a 12-year wave hindcast covering the period February 2006 - December 2017. It consists of hourly wave parameters at 1/24º horizontal resolution covering the Mediterranean Sea and extending up to -18.125ºW into the Atlantic Ocean. It is produced using the set-up and configuration of the Q3/2017 version of the Med-waves (Med-MFC wave component) analysis and forecast system described below.

Med-waves is based on the state-of-the-art third-generation wave model WAM Cycle 4.5.4 (Günther and Behrens, 2012) which is a modernized and improved version of the well-known and extensively used WAM Cycle 4 wave model (WAMDI Group, 1988; Komen et al., 1994). Cycle 4.5.4 has been released during MyWave ("A pan - European concerted and integrated approach to operational wave modelling and forecasting – a complement to GMES MyOcean services") EU FP7 Research Project and is freely available to the entire research and forecasting community.

WAM solves the wave transport equation explicitly without any presumption on the shape of the wave spectrum. Its source terms include the wind input, whitecapping dissipation, nonlinear transfer and bottom friction. The wind input term is adopted from Snyder et al. (1981). The whitecapping dissipation term is based on Hasselmann (1974) whitecapping theory. The wind input and whitecapping dissipation source terms of the present cycle of the wave model are a further development based on Janssen´s quasi-linear theory of wind-wave generation (Janssen, 1989; Janssen, 1991). The nonlinear transfer term is a parameterization of the exact nonlinear interactions as proposed by Hasselmann and Hasselmann (1985) and Hasselmann et al., (1985). Lastly, the bottom friction term is based on the empirical JONSWAP model of Hasselmann et al. (1973).

The Med-waves set-up includes a coarse grid domain with a resolution of 1/6º covering the North Atlantic Ocean from 75ºW to 10ºE and from 10ºN to 70ºN and a nested fine grid domain with a resolution of 1/24º covering the Mediterranean Sea from 18.125ºW to 36.2917ºE and from 30.1875ºN to 45.9792ºN. The areas covered by the two grids are shown in Figure 2.

The bathymetric map has been constructed using the GEBCO bathymetric data set (GEBCO, 2016) for the Mediterranean Sea model and the ETOPO2 data set (NGDC, 2006) for the North Atlantic model. In both cases mapping on the model grid was done using bi-linear interpolation accompanied by some degree of isotropic laplacian smoothing.

The Mediterranean Sea model receives from the North Atlantic model full wave spectrum at 3-hourly intervals at its Atlantic Ocean open boundary. The latter model is considered to have all of its four boundaries closed assuming no wave energy propagation from the adjacent seas. This assumption is readily justified for the north and west boundaries of the North Atlantic model considering the adjacent topography which restricts the development and propagation of swell into the model domain. The choice of the south boundary location is less obvious and is based on a number of studies which agree that no important swell energy is expected to propagate northwards from geographical areas south of 10ºN. Specifically, according to Semedo et al. (2011), a swell front present in all seasons can be identified in the Atlantic Ocean within the latitude band from 15ºS (Dec-Jan-Feb) to 15ºN (Jun-Jul-Aug). Young (1999) suggests this swell front never migrates north of the equator. The relatively narrow geometry of the Atlantic restricts propagation of Southern Ocean swell into the Northern Hemisphere. According to Alves (2006) storms within the extratropical South Atlantic ocean (below 40ºS) typically propagate to the east spreading swell energy to the Indian Ocean. As for the Atlantic tropical areas, storms rarely evolve in the south band (between 20ºS and the equator) while in the north tropical band (between the equator and 20ºN) summer storms move mostly westwards. During

winter, the north tropical band can be affected by eastward propagating North Atlantic extratropical storms generating swells that propagate to the southeast (Alves, 2006).

The wave spectrum is discretized using 32 frequencies, which cover a logarithmically scaled frequency band from 0.04177 *Hz* to 0.8018 *Hz* (covering wave periods ranging from approximately 1s to 24s) at intervals of df/f = 0.1, and 24 equally spaced directions (15 degrees bin).

The Mediterranean model runs in shallow water mode considering wave refraction due to depth and currents in addition to depth induced wave breaking. The North Atlantic model runs in deep water mode with wave refraction due to currents only. The North Atlantic model additionally considers wave energy damping due to the presence of sea ice. A model grid point is considered to be a sea ice point if the ice fraction at that point exceeds 60%. At all sea ice points the wave energy is set to zero.

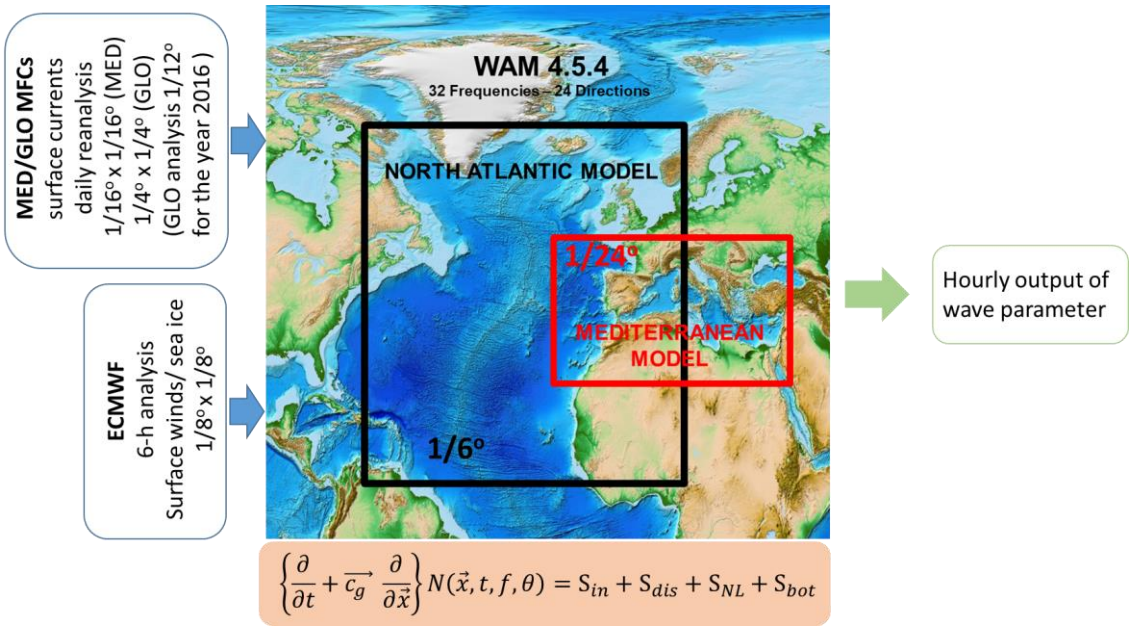

Figure 2: Bathymetry and model configuration of Med-waves

Following the European Centre For Medium-Range Weather Forecasts (ECMWF, 2015), the tunable whitecapping dissipation coefficients C_{ds} and δ have been altered from their default values. Specifically, the values of C_{ds} = 1.33 (C_{ds} = 2.1 default) and C_{ds} = 1.8 have been adopted for the Mediterranean and Atlantic model respectively whilst δ = 0.5 (δ = 0.6 default) have been adopted for both models. The aim of this tuning is to produce results which are in good agreement with data on fetch-limited growth and with data on the dependence of the surface stress on wave age.

To produce the Med-MFC multi-year wave hindcast, the aforementioned models are forced by ECMWF 6-hourly analysis 10m wind fields that are disseminated at a horizontal resolution of 1/8° but have a changing nominal horizontal resolution which is 0.225º for the period 2006-2010, 0.141º for the period 2010-2016 and 0.07º since March 2016. The wind is bi-linearly interpolated onto the model grids. ECMWF 6-hourly analysis sea ice coverage at the same horizontal resolution as the winds is also input in the Atlantic model. With respects to currents forcing, the Mediterranean Sea model is forced by daily averaged reanalysis surface currents obtained from the CMEMS Med MFC (Q1/2019) at 1/16º resolution. The North Atlantic model is forced by daily averaged reanalysis surface currents obtained from the CMEMS Global MFC (Q3/2016) at 1/4º resolution for the years 2006-2015 and by daily

averaged analysis surface currents obtained from the CMEMS Global MFC (Q2/2018) at 1/12º resolution for the years 2016-2017. A schematic of the Med-MFC wave hindcast system is shown in Figure 2.

The Med-MFC wave hindcast consists of hourly wave fields over the Mediterranean Sea at 1/24º horizontal resolution. These wave fields correspond either to wave parameters computed by integration of the total wave spectrum or to wave parameters computed using wave spectrum partitioning. In the latter case the complex wave spectrum is partitioned into wind sea, primary and secondary swell. Wind sea is defined as those wave components that are subject to wind forcing while the remaining part of the spectrum is termed swell. Wave components are considered to be subject to wind forcing when

$$c \leq 1.2 \times 28\, u_* \cos(\theta - \varphi)$$

where c is the phase speed of the wave component, u_* is the friction velocity, θ is the direction of wave propagation and ϕ is the wind direction. As the swell part of the wave spectrum can be made up of different swell systems with quite distinct characteristics it is further partitioned into the two most energetic wave systems, the so called primary and secondary swell. Swell partitioning is done following the method proposed by Gerling (1992) which finds the lowest energy threshold value at which upper parts of the spectrum get disconnected with the process repeated until primary and secondary swell is detected.

II.3 Upstream data and boundary condition of the WAM model

The CMEMS Med-MFC wave hindcast system uses the following upstream datasets:

1. Atmospheric forcing: NWP (Numerical Weather Prediction) 6-h, operational analysis fields from ECMWF, distributed by the Italian National Meteo Service (USAM/CNMA). Nominal resolutions: 0.225º from Feb 2006 to Jan 2010, 0.141º from Jan 2010 to Mar 2016 and 0.07º from Mar 2016 to Dec 2016. Dissemination resolution: 1/8 º.
2. Surface currents forcing: GLOBAL_REANALYSIS_PHY_001_025 daily averages at 1/4º for years 2006-2015 and GLOBAL_ANALYSIS_FORECAST_PHY_001_024 daily averages at 1/12º for years 2016-2017 (Atlantic model grid forcing); MEDSEA_REANALYSIS_PHY_006_004 daily averages at 1/16º (Mediterranean model grid forcing)
3. Sea-ice cover: daily analysis fields from ECMWF at the same nominal and dissemination resolution as the ECMWF winds, distributed by the Italian National Meteo Service (USAM/CNMA).

III VALIDATION FRAMEWORK

In order to evaluate and assure the quality of the MEDSEA_HINDCAST_WAV_006_012 product of the CMEMS Med-MFC multi-year wave hindcast released in Q1/2019, hindcast wave parameters were compared to observations, focusing on model output quality in the Mediterranean Sea.

The wave parameters that have been qualified through their comparison with observations include:

- ✓ spectral significant wave height (Hm0) [SWH]
- ✓ spectral moments (0,2) wave period (Tm02) [MWP]

The remaining hindcast wave parameters included in the CMEMS Med-MFC waves multi-year product are not qualified against observational data. This is mainly because there are no relevant observations or because the existing observations are not suited for a robust validation either because of limited data availability or because of data ambiguities (e.g. highly spiky variation). In most of the cases, the quality of these wave parameters is inferred from the quality of those parameters that are thoroughly compared with observations. A valid range, based on climatology and/or expert knowledge, is assigned to each wave parameter.

The observations against which modelled wave parameters are compared to include:

- quality-controlled in-situ observations from moored wave buoys obtained from the CMEMS INSITU_MED_NRT_OBSERVATIONS_013_035 dataset, available through the CMEMS INS-TAC
- in-situ observations from moored Italian wave buoys obtained from ISPRA, Italy
- satellite altimeter observations from a merged altimeter wave height database setup at CERSAT - IFREMER.

In-situ observations come from 41 wave buoys in the Mediterranean Sea.

Figure 3 depicts their location and unique ID code. All depicted wave buoys have at least 2 'full'-years of measurements within the base hindcast period 2006-2015 (Q3/2017). A year of measurements is considered to be 'full' if at least 200 model-buoy collocations are obtained for winter, summer, and either spring or autumn, i.e. the year-long wave regime is sufficiently represented. Wave buoys

depicted in yellow have at least 5 consecutive 'full'-years of measurements within the base period. Hindcast-long (2006-2015) statistics of SWH and MWP have been computed for each of the wave buoys depicted in Figure 3 (buoys 61001 and 61002 do not measure MWP) using all available measurements. Equivalent hindcast-long statistics for the entire Mediterranean Sea have been computed using merged observations from the 25 wave buoys in yellow considering only 'full' consecutive years of measurements. In addition, based on the same data (buoy 61188 replaced by 61289), yearly statistics over the entire Q1/2019 hindcast period (2006-2017) have been calculated. Such statistics are provided for the full Mediterranean Sea as well as for individual wave buoy groups generated by merging wave buoy observations obtained over the same consecutive years, over a specified region. The wave buoy groups generated for the computation of yearly statistics are presented in Table 3.

To collocate model output and buoy measurements, in space, model output was taken at the grid point nearest to the buoy location. In time, buoy measurements within a time window of ± 1 hr from model output times at 3-hr intervals (0, 3, 6, ..., etc) were averaged. Prior to model-buoy collocation, the in-situ observations were filtered so as to remove those values accompanied by a bad quality flag (Quality Flags included in the data files provided by the INS-TAC). After collocation, visual inspection of the data was carried out, which led to some further filtering of spurious data points. In addition, MWP data below 2 sec were omitted from the statistical analysis, since 0.5 Hz (T = 2 sec) is a typical cut-off frequency for wave buoys.

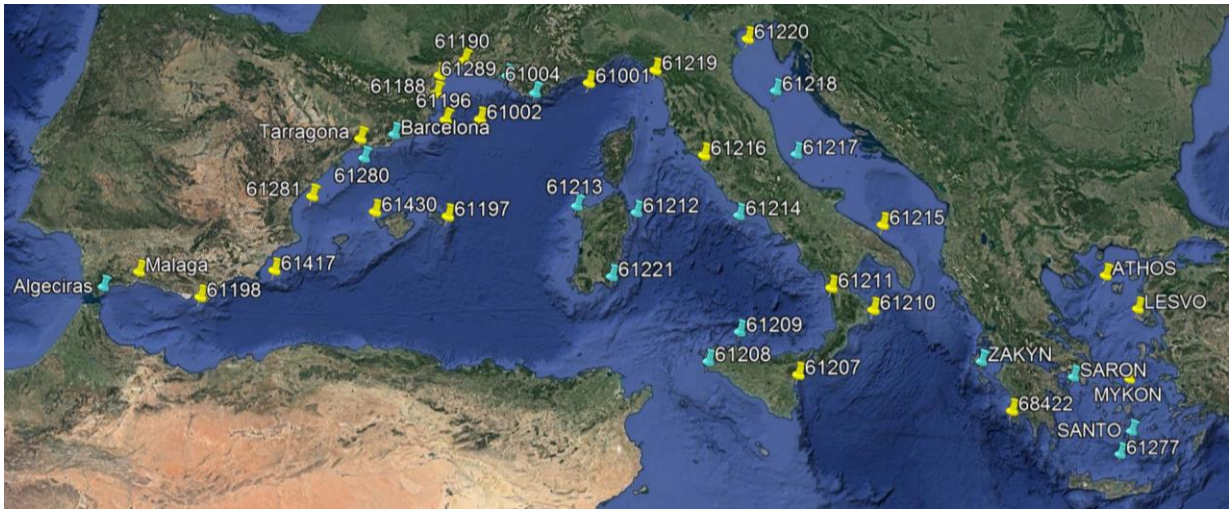

Figure 3: Wave buoys locations

Group Name	Wave buoys	Period of data
ES offshore	61198, 61417, 61281, 61280, 61430, 61197, 61196	2007-2017
ES coastal	Malaga, Tarragona	2007-2017
ES	All ES sub-groups	2007-2017
FR offshore	61001, 61002	2007-2017
FR coastal	61190, 61191, 61289	2011-2017
IT Tyrrhenian	61211, 61216, 61219	2010 - 2014
IT Ionian	61210, 61207	2010 - 2014
IT Adriatic	61220, 61215	2010 - 2014
IT	All IT sub-groups	2010 - 2014

GR Ionian	68422	2008-2015
GR Aegean	ATHOS, LESVO, MYKON	2007-2012

Table 3: Wave buoy groups: ES = Spanish, FR = French, IT = Italian, GR = Greek.

Satellite observations of SWH are from 7 satellite missions, shown in Table 4**Erreur ! Source du renvoi introuvable.**. Satellite observations of wind speed, U10, used to validate the ECMWF forcing winds, come from a sub-set of these missions (excluding Cryosat2 and Saral). All satellite SWH and U10 observations have been filtered and corrected (Queffeulou and Croizé-Fillon, 2017). Similarly to the model-buoy comparisons, hindcast-long (2006-2015, Q3/2017) and yearly statistics (2006-2016, Q1/2018 – year 2017 was omitted due to satellite data inadequacy, as explained in Section I.3) have been computed for individual satellites and merged satellite observations. Yearly statistics have been obtained using satellite missions with at least 3 consecutive full-years of measurements. Statistics were produced for the full Mediterranean Sea and for the individual sub-regions defined in Figure 1 (or aggregations of them).

Satellite	Period of data
Ers2	01/2008 - 07/2011
Envisat	01/2006 - 04/2012
Jason1	01/2006 - 06/2013
Jason2	07/2008 - 12/2016
GeosatFO	01/2006 - 09/2008
Cryosat2	07/2010 - 12/2016
Saral	03/2013 - 12/2016

Table 4: Satellite missions

To collocate model output and satellite observations the former were interpolated in time and space to the individual satellite tracks. For each track, corresponding to one satellite pass, along-track pairs of satellite measurements and interpolated model output were averaged over ~50 km (0.5°) grid cells, centered at grid points of the forcing wind model (0.125° x 0.125°). This averaging is intended to remove any spatial correlation present in successive 1 Hz (~7 km) observations and/or in neighbouring model grid output (Queffeulou, personal communication).

Metrics that are commonly applied to assess numerical model skill and are in alignment with the recommendations of the EU FP7 project MyWave (A pan-European concerted and integrated approach to operational wave modelling and forecasting – a complement to GMES MyOcean services, 2012-2014) have been used to qualify the Med-MFC multi-year wave hindcast within the Mediterranean Sea. These include the RMSD, BIAS, Scatter Index (SI), Pearson Correlation Coefficient (CORR), and best-fit Slope (LR_SLOPE). The SI, defined here as the standard deviation of model-observation differences relative to the observed mean, being dimensionless, is more appropriate to evaluate the relative closeness of the model output to the observations at different locations compared with the RMSD which is representative of the size of a 'typical' model-observation difference. The LR_SLOPE corresponds to a best-fit line forced through the origins (zero intercept). In addition to the aforementioned core metrics, merged Density Scatter and Quantile-Quantile (QQ) plots are provided.

The full set of metrics used in the qualification of the Med-MFC multi-year wave hindcast is defined in **Erreur ! Source du renvoi introuvable.**.

Name	Description	Wave parameter	Supporting reference dataset	Quantity
Evaluation of Med-MFC multi-year wave product using in-situ observations (Full MED)				
SWH-H-CLASS2-MOOR-<STAT>-10YR-MED	Comparison to wave buoy significant wave height	Spectral significant wave height (Hm0)	- INSITU_MED_NRT_OBSERVATIONS_013_035 - wave buoy data from ISPRA, Italy	RMSD, SI, BIAS, CORR, LR-SPOPE respectively between observations and hindcast, for all Med, for the entire Q3/2017 MYP period (2006-2015) and seasonally
MWP-H-CLASS2-MOOR-<STAT>-10YR-MED	Comparison to wave buoy mean wave period	Spectral moments (0,2) wave period (Tm02)	- INSITU_MED_NRT_OBSERVATIONS_013_035 - wave buoy data from ISPRA, Italy	RMSD, SI, BIAS, CORR, LR-SPOPE respectively between observations and hindcast, for all Med, for the entire Q3/2017 MYP period (2006-2015) and seasonally
SWH-H-CLASS2-MOOR-QQ-10YR-MED SWH-H-CLASS2-MOOR-SCATTER-10YR-MED	Comparison to wave buoy significant wave height	Spectral significant wave height (Hm0)	- INSITU_MED_NRT_OBSERVATIONS_013_035 - wave buoy data from ISPRA, Italy	Merged Quantile-Quantile and Scatter plots between observations and hindcast, for all Med, for the entire Q3/2017 MYP period (2006-2015)
MWP-H-CLASS2-MOOR-QQ-10YR-MED MWP-H-CLASS2-MOOR-SCATTER-10YR-MED	Comparison to wave buoy mean wave period	Spectral moments (0,2) wave period (Tm02)	- INSITU_MED_NRT_OBSERVATIONS_013_035 - wave buoy data from ISPRA, Italy	Merged Quantile-Quantile and Scatter plots between observations and hindcast, for all Med, for the entire Q3/2017 MYP period (2006-2015)
SWH-H-CLASS2-MOOR-<STAT>-YR-MED	Comparison to wave buoy significant wave height	Spectral significant wave height (Hm0)	- INSITU_MED_NRT_OBSERVATIONS_013_035 - wave buoy data from ISPRA, Italy	Time-series of yearly and seasonal values of RMSD, SI, BIAS, CORR, LR-SPOPE respectively between observations and hindcast, for all Med.
MWP-H-CLASS2-MOOR-<STAT>-YR-MED	Comparison to wave buoy mean wave period	Spectral moments (0,2) wave period (Tm02)	- INSITU_MED_NRT_OBSERVATIONS_013_035 - wave buoy data from ISPRA, Italy	Time-series of yearly and seasonal values of RMSD, SI, BIAS, CORR, LR-SPOPE respectively between observations and hindcast, for all Med
SWH-H-CLASS2-MOOR-PERC99-YR-MED	Comparison to wave buoy significant wave height	Spectral significant wave height (Hm0)	- INSITU_MED_NRT_OBSERVATIONS_013_035 - wave buoy data from ISPRA, Italy	Time series of yearly 99th percentile differences between hindcast and observations, for all Med

Table 5: List of metrics for the Med-MFC multi-year wave hindcast evaluation using in-situ and satellite observations (continues overleaf).

Evaluation of Med-MFC multi-year wave product using in-situ observations (at buoy locations or for wave buoy groups)				
SWH-H-CLASS2-MOOR-<STAT>-10YR-<MOORING ID>	Comparison to wave buoy significant wave height	Spectral significant wave height (Hm0)	- INSITU_MED_NRT_OBSERVATIONS_013_035 - wave buoy data from ISPRA, Italy	RMSD, SI, BIAS, CORR, LR_SLOPE respectively between observations and hindcast, for each wave buoy separately, for the entire Q3/2017 MYP period (2006-2015)
MWP-H-CLASS2-MOOR-<STAT>-10YR-<MOORING ID>	Comparison to wave buoy mean wave period	Spectral moments (0,2) wave period (Tm02)	- INSITU_MED_NRT_OBSERVATIONS_013_035 - wave buoy data from ISPRA, Italy	RMSD, SI, BIAS, CORR, LR_SLOPE respectively between observations and hindcast, for each wave buoy separately, for the entire Q3/2017 MYP period (2006-2015)
SWH-H-CLASS2-MOOR-QQ-10YR-<MOORING ID> SWH-H-CLASS2-MOOR-SCATTER-10YR-<MOORING ID>	Comparison to wave buoy significant wave height	Spectral significant wave height (Hm0)	- INSITU_MED_NRT_OBSERVATIONS_013_035 - wave buoy data from ISPRA, Italy	Merged Quantile-Quantile and Scatter plots between observations and hindcast, for each wave buoy separately, for the entire Q3/2017 MYP period (2006-2015)
MWP-H-CLASS2-MOOR-QQ-10YR-<MOORING ID> MWP-H-CLASS2-MOOR-SCATTER-10YR-<MOORING ID>	Comparison to wave buoy mean wave period	Spectral moments (0,2) wave period (Tm02)	- INSITU_MED_NRT_OBSERVATIONS_013_035 - wave buoy data from ISPRA, Italy	Merged Quantile-Quantile and Scatter plots between observations and hindcast, for each wave buoy separately, for the entire Q3/2017 MYP period (2006-2015)
SWH-H-CLASS2-MOOR-<STAT>-YR-<MOORINGS GROUP ID>	Comparison to wave buoy significant wave height	Spectral significant wave height (Hm0)	- INSITU_MED_NRT_OBSERVATIONS_013_035 - wave buoy data from ISPRA, Italy	Time-series of yearly values of RMSD, SI, BIAS, CORR, LR_SLOPE respectively between observations and hindcast, for individual wave buoy groups
MWP-H-CLASS2-MOOR-<STAT>-YR-<MOORINGS GROUP ID>	Comparison to wave buoy mean wave period	Spectral moments (0,2) wave period (Tm02)	- INSITU_MED_NRT_OBSERVATIONS_013_035 - wave buoy data from ISPRA, Italy	Time-series of yearly values of RMSD, SI, BIAS, CORR, LR_SLOPE respectively between observations and hindcast, for individual wave buoy groups

Table 6: (continued) List of metrics for the Med-MFC multi-year wave hindcast evaluation using in-situ and satellite observations.

Evaluation of Med-MFC multi-year wave product using satellite observations (full MED)				
SWH-H-CLASS4-ALT-<STAT>-10YR-MED	Comparison to altimeter significant wave height	Spectral significant wave height (Hm0)	Merged altimeter wave height database from CERSAT – IFREMER	RMSD, SI, BIAS, CORR, LR-SPOPE respectively between observations and hindcast, for all Med, for the entire Q3/2017 MYP period (2006-2015) and seasonally
SWH-H-CLASS4-ALT-QQ-10YR-MED SWH-H-CLASS4-ALT-SCATTER-10YR-MED	Comparison to altimeter significant wave height	Spectral significant wave height (Hm0)	Merged altimeter wave height database from CERSAT – IFREMER	Merged Quantile-Quantile and Scatter plots between observations and hindcast, for all Med, for the entire Q3/2017 MYP period (2006-2015)
SWH-H-CLASS4-ALT-<STAT>-YR-MED	Comparison to altimeter significant wave height	Spectral significant wave height (Hm0)	Merged altimeter wave height database from CERSAT – IFREMER	Time-series of yearly and seasonal values of RMSD, SI, BIAS, CORR, LR-SPOPE respectively between observations and hindcast, for all Med
SWH-H-CLASS4-ALT-PERC99-YR-MED	Comparison to altimeter significant wave height	Spectral significant wave height (Hm0)	Merged altimeter wave height database from CERSAT – IFREMER	Time series of yearly 99th percentile differences between hindcast and observations, for all Med
Equivalent metrics are produced for individual satellite missions				
Evaluation of Med-MFC multi-year wave product using satellite observations (MED sub-regions)				
SWH-H-CLASS4-ALT-<STAT>-10YR-<REGION>	Comparison to altimeter significant wave height	Spectral significant wave height (Hm0)	Merged altimeter wave height database from CERSAT - IFREMER	RMSD, SI, BIAS, CORR, LR_SLOPE respectively between observations and hindcast, for individual Med sub-regions, for the entire Q3/2017 MYP period (2006-2015)
SWH-H-CLASS4-ALT-QQ-10YR-<REGION> SWH-H-CLASS4-ALT-SCATTER-10YR-<REGION>	Comparison to altimeter significant wave height	Spectral significant wave height (Hm0)	Merged altimeter wave height database from CERSAT - IFREMER	Merged Quantile-Quantile and Scatter plots between observations and hindcast, for individual Med sub-regions, for the entire Q3/2017 MYP period (2006-2015)
SWH-H-CLASS4-ALT-<STAT>-YR-<REGION>	Comparison to altimeter significant wave height	Spectral significant wave height (Hm0)	Merged altimeter wave height database from CERSAT - IFREMER	Time-series of yearly values of RMSD, SI, BIAS, CORR, LR_SLOPE respectively between observations and hindcast, for individual Med sub-regions

Table 7: (continued) List of metrics for the Med-MFC multi-year wave hindcast evaluation using in-situ and satellite observations.

IV VALIDATION RESULTS

IV.1 Significant wave height

Comparison with in-situ observations

Table 8 shows results of the comparison between hindcast SWH (model data) and in-situ observations of SWH (reference data), for the Mediterranean Sea as a whole, for the entire Q3/2017 hindcast period (2006-2015) and seasonally. The observations used are from the wave buoys depicted in

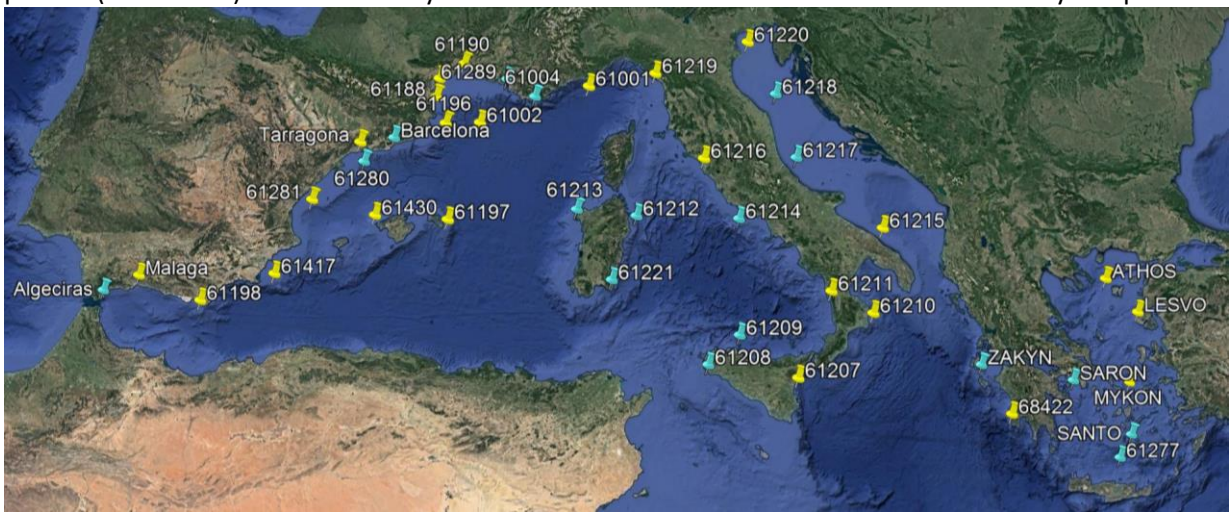

Figure 3 in yellow. In the table, "Entries" refers to the number of model-buoy collocation pairs, i.e. to the sample size available for the computation of the relevant statistics, $\overline{R}$ is the mean reference value, $\overline{M}$ is the mean model value, STD R and STD M are the standard deviations of the reference and model data respectively. The remaining quantities are the qualification metrics defined in the previous section. Figure 4 is the respective merged QQ-Scatter plot for the full hindcast period. In the figure, the QQ-plot is depicted with black crosses. Also shown are the best fit line forced through the origin (red solid line) and the 45° reference line (red dashed line).

MED	ENTRIES	$\overline{R}$ (m)	$\overline{M}$ (m)	STD R (m)	STD M (m)	RMSD (m)	SI	BIAS (m)	CORR	LR_SLOPE
Full period	458246	0.88	0.86	0.74	0.77	0.23	0.27	-0.02	0.95	0.98
Winter	109268	1.12	1.09	0.9	0.93	0.27	0.24	-0.03	0.96	0.98
Spring	112490	0.88	0.87	0.72	0.74	0.23	0.26	-0.01	0.95	0.98
Summer	121095	0.63	0.63	0.47	0.51	0.19	0.30	0.00	0.93	1.00
Autumn	115393	0.92	0.89	0.75	0.78	0.24	0.26	-0.04	0.95	0.97

Table 8: Hindcast SWH evaluation against wave buoys' SWH, for the full Mediterranean Sea, for the full Q3/2017 hindcast period and seasonally (2006-2015). Relevant metrics from **Erreur ! Source du renvoi introuvable.**: SWH-H-CLASS2-MOOR-<STAT>-10YR-MED.

Table 8 shows that the typical difference between model output and observations (RMSD) varies from 0.19 m in summer to 0.27 m in winter. However, the scatter in summer (0.3) is 6% higher than the

scatter in winter (0.24) whilst a lower correlation coefficient is associated with the former season. This suggests that the model follows better the observations in 'stormy' conditions, with well-defined patterns and higher waves. A similar conclusion has been derived by other studies (Cavaleri and Sclavo, 2006; Ardhuin et al., 2007; Bertotti et al., 2013) with respect to wind and wave modelling performance in the Mediterranean Sea. Spring and autumn values of the aforementioned metrics are alike and lie in between summer and winter values. A small negative BIAS is observed, reaching 4.5% in autumn (BIAS/$\overline{R}$) and being 0% in summer. Similarly, LR_SLOPES vary from 0.97 in autumn to unity in summer. These values are indicative of an underestimation of the wave height in the Mediterranean Sea by the model, a result which is in agreement with the results of a number of hindcast, operational or pre-operational wave modelling studies for the Mediterranean Sea (e.g. Ratsimandresy et al., 2008; Martínez-Asensio et al., 2013; Bidlot, 2015; Donatini et al., 2015) and is linked to an underestimation of the wind speed by the ECMWF forcing wind model (see Figure 12). Overall, the spring statistics are the ones closest to the full hindcast period statistics for the Mediterranean Sea.

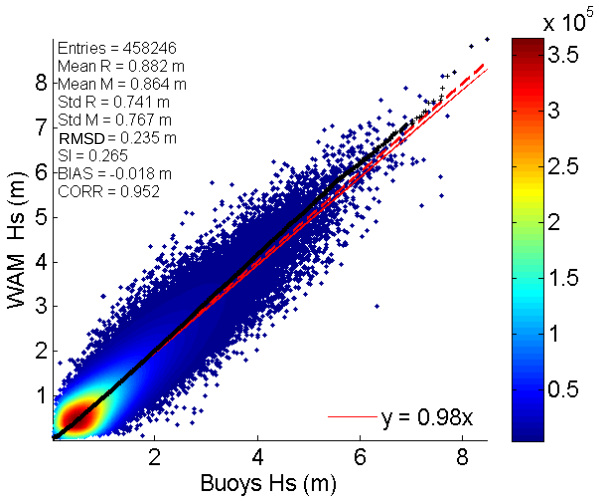

Figure 4: QQ-Scatter plots of hindcast SWH (Hs) versus wave buoys' observations, for the full Mediterranean Sea, for the full Q3/2017 hindcast period (2006-2015): QQ-plot (black crosses), 45° reference line (dashed red line), least-squares best fit line (red line). Relevant metrics from **Erreur ! Source du renvoi introuvable.**: SWH-H-CLASS2-MOOR-QQ-10YR-MED, SWH-H-CLASS2-MOOR-SCATTER-10YR-MED.

Figure 4 depicts the pattern of the agreement between hindcast and observed SWH for different SWH value ranges. The figure reveals that the SWH underestimation by the model is mainly occurring for wave heights below 2 m and is rather small. A more pronounced overestimation of SWH is actually observed above this value. Nevertheless, the QQ-plot shows that, in both cases, waves of a specific wave height have a very similar probability of occurrence in the hindcast and in the observations.

Figure 5 shows results of the comparison between hindcast SWH and in-situ observations for each of the wave buoys depicted in

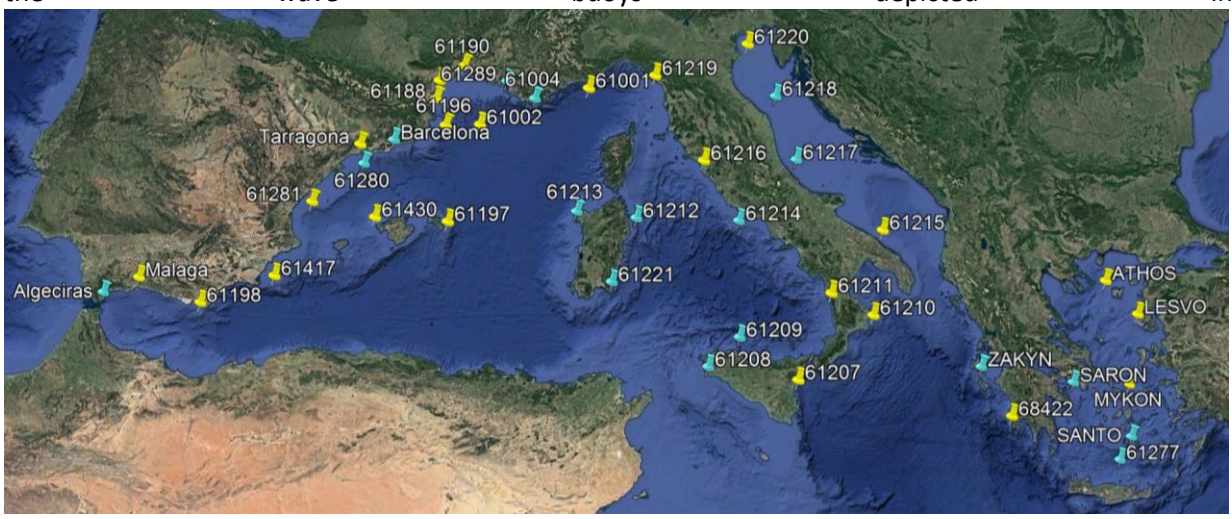

Figure 3 (from west to east). Tabulated results are included in the Appendix (Table A1). The figure facilitates the visualization and interpretation of the relative performance of the wave model at the different locations. To be able to readily compare the pattern of variation of the different metrics at the different locations the absolute BIAS and the CORR deviation from unity are plotted in the bottom plot of Figure 5. Original values of BIAS and LR_SLOPE are shown in the middle plot. For convenience, a map of the wave buoy locations is included in the figure (top).

Figure 5 (and Table A1) reveals that the typical difference (RMSD) at the different buoy locations varies from 0.16 m (Tarragona) to 0.4 m (61004). SI, which does not follow the RMSD variation, varies from 0.18 at offshore buoy 61002 to 0.4 at buoy 61220 in the North Adriatic Sea. In general, SI values above the mean value for the whole Mediterranean Sea (0.27) are obtained at wave buoys that are sheltered by land masses on their west north-west (e.g. western French coastline and eastern coastline of mainland Italy), are near the coast (e.g. coastal Spanish buoys) and/or are surrounded by complex topography (e.g. 61004, 61221, Adriatic and Aegean Seas). In the first case, deterioration of wave model performance is because the resolution of the forcing wind model is not capable of well reproducing the fine interaction between the prevailing north-northwesterly winds in the northern Mediterranean Sea and the complex orography sheltering the northern Mediterranean coastline. In the second case, when the buoys are located only a few kilometers from the coastline and the wind is blowing from the coast (e.g. 61188, Algeciras, Malaga, Tarragona) the approximation of the wave model grid size can lead to non-negligible fetch differences (e.g. Ardhuin et al., 2007; Cavaleri and

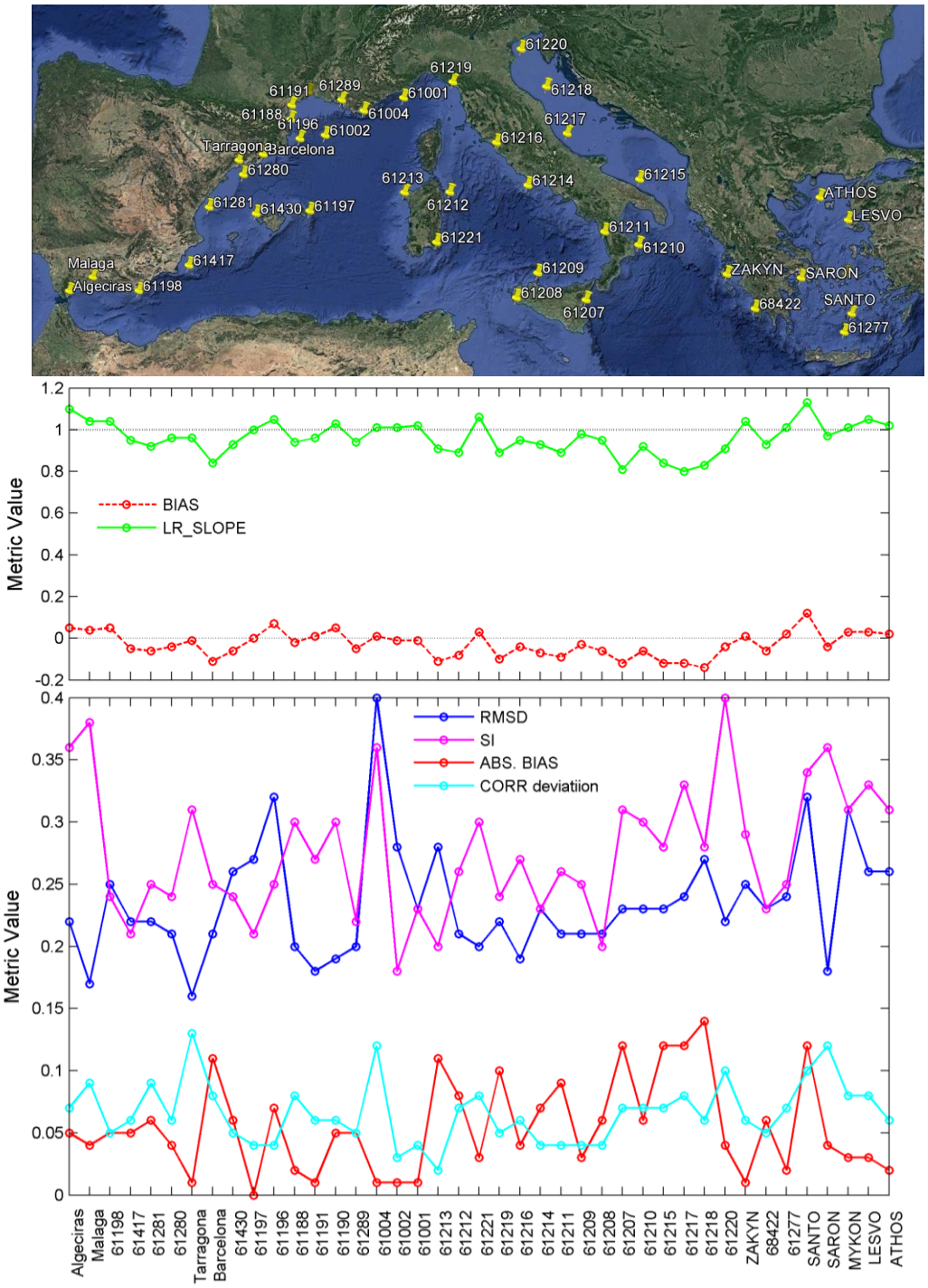

Figure 5: SWH metrics (middle, bottom) at buoy locations (top) for the full Q3/2017 hindcast period (2006-2015). Plots display metrics starting from the western buoy location and moving eastwards. Bottom plot: CORR deviations from unity are shown. Relevant metrics from Table 5: SWH-H-CLASS2-MOOR-<STAT>-10YR-<MOORING ID>.

Sclavo, 2006). Finally, in the latter case, it is also the spatial resolution of the wave model that is not adequate to resolve the fine bathymetric features. In general, the more close the location to the coastline (e.g. Malaga) and/or the more complex the surrounding topography (e.g. SARON) the poorer the model performance expected (e.g. Cavaleri and Sclavo, 2006; Bertotti et al., 2013; Zacharioudaki et al., 2015). The correlation coefficient (CORR) largely follows the pattern of variation of the SI. It ranges from 0.87 at the coastal buoy of Tarragona to 0.98 at a location west of Sardinia (61213) which is well exposed to the prevailing north-westerly winds in the region. BIAS varies from -0.14 m at buoy 61218 in the Adriatic Sea to 0.12 m at buoy SANTO in the Aegean Sea with positive BIAS being mostly below 0.05. BIAS is mainly negative indicating an underestimation of the observed wave height by the model. Nevertheless, as seen in Figure 4 and as it will be further explained in the following paragraph model bias varies throughout the wave height range and from location to location. The pattern of variation of LR_SLOPE (not shown) is close to the pattern of variation of BIAS with values that range from 0.8 (61217) to 1.13 (SANTO).

Figure 6, similarly to Figure 4, shows the QQ-Scattter plots of hindcast SWH versus measured SWH at four buoy locations, exhibiting model performance over the different wave height ranges. Based on the results at these four locations, an attempt will be made to describe the different behaviour of the wave model at the different wave buoy locations in the Mediterranean Sea shown in

Figure 3. Thus, the top right plot shows results at buoy location 61002. This is a very well exposed offshore wave buoy where model results are optimal. In particular, the scatter of the data is small with QQ crosses and best-fit line laying very close to the reference line. A small model underestimate is observed for wave heights below 2 m and a small overestimate for bigger waves. The behaviour of the model at this location is expected to be representative of its performance at well-exposed offshore sites. Indeed, a similar distribution is found at other relatively offshore locations (e.g. 61417, 61196, 61001, ATHOS). The point where model passes from underestimate to overestimate may be shifted. Also, over the lower wave height range the model may diverge more or converge better to the observations whilst over the higher wave height range, especially at high values, model may show a larger overestimation. A reversed distributional variation, found in only few coastal locations (61190, 61191) may be seen in the bottom right plot for location 61190 offshore the French coastline. A more typical distribution near the coast is the one shown at the top right plot for location 61207, offshore Catania in Italy, backed on the north-west by the mount Etna. It is seen that model underestimation occurs throughout the measured SWH range except from the very highest percentiles of SWH where model overestimation is observed. This scatter distribution is very common amongst coastal wave

buoys that are facing east (e.g. 61188, eastern Italian coastline) but also at wave buoys that are well-exposed to westerly fetches but are sheltered by land on their east (e.g. 61430, 61213, 61211, 68422). This wave underestimation is most probably related to considerable wind underestimation by the forcing wind model at these coastal locations sheltered by complex topography (e.g. Ardhuin et al., 2007). The bottom left plot corresponds to buoy SANTO in the Aegean Sea. There, the model overestimates the observed SWH over most of the SWH range, even more so in the upper end of this range. Considerable model overestimation, mostly over the middle and higher SWH ranges, is observed at all wave buoys associated with unresolved bathymetric features in their surroundings (e.g. 61221, SARON). A larger scatter is often associated with such locations. Model overestimation throughout the SWH range is also observed in the Alboran Sea (e.g. 61198) and is part of a general model overestimation east and west of the Gibraltar Straight as it will be shown later in the comparison with the satellite observations.

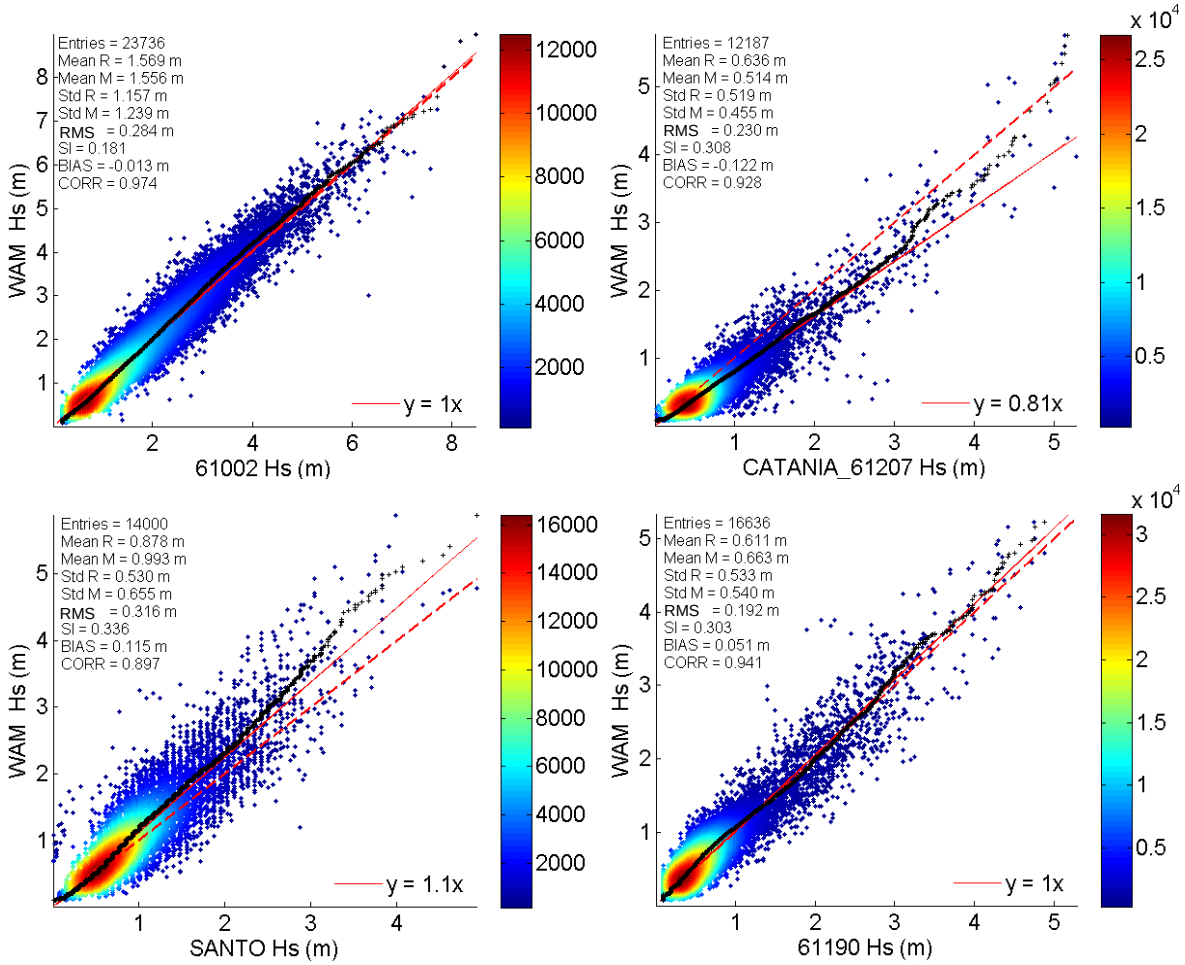

Figure 6: QQ-Scatter plots of hindcast SWH (Hs) versus wave buoy observations at specific wave buoy locations, for the full Q3/2017 hindcast period (2006-2015): QQ-plot (black crosses), 45° reference line (dashed red line), least-squares best fit line (red line). Relevant metrics from **Erreur ! Source du renvoi introuvable.**: SWH-H-CLASS2-MOOR-QQ-10YR-<MOORING ID>, SWH-H-CLASS2-MOOR-SCATTER-10YR-<MOORING ID>.

Up to now, the quality of the Med-MFC multi-year wave hindcast has been examined through the production of long-term metrics considering the entire Q3/2017 hindcast period (2006-2015). In the

following, metric values are computed on a yearly basis (2006-2017, Q1/2019) allowing exploration of their inter-annual variability. This type of analysis is useful for the identification of any inconsistencies in hindcast quality in time and for non-regression testing in relation to future updates of the product. It also shows how the time variation of metric values is strongly dependent on the set of observations available for the comparisons. Thus, Figure 7 shows yearly values of SWH metrics for the full Mediterranean Sea and for the wave buoy groups defined in Table 3 in Section III. In parallel, Figure 8 shows the number of yearly model-buoy collocation pairs available per wave buoy group. In addition, Figure 9 shows the inter-annual seasonal variability (winter and summer) of the metrics for the full Mediterranean Sea. Finally, to obtain an insight of how the model simulates the extreme wave events in the Mediterranean Sea, yearly values of the differences between hindcast and observed 99th percentile of SWH for the full Mediterranean Sea are plotted in Figure 10 together with the maximum and minimum signed differences found in the basin when considering equivalent values at the individual wave buoy locations.

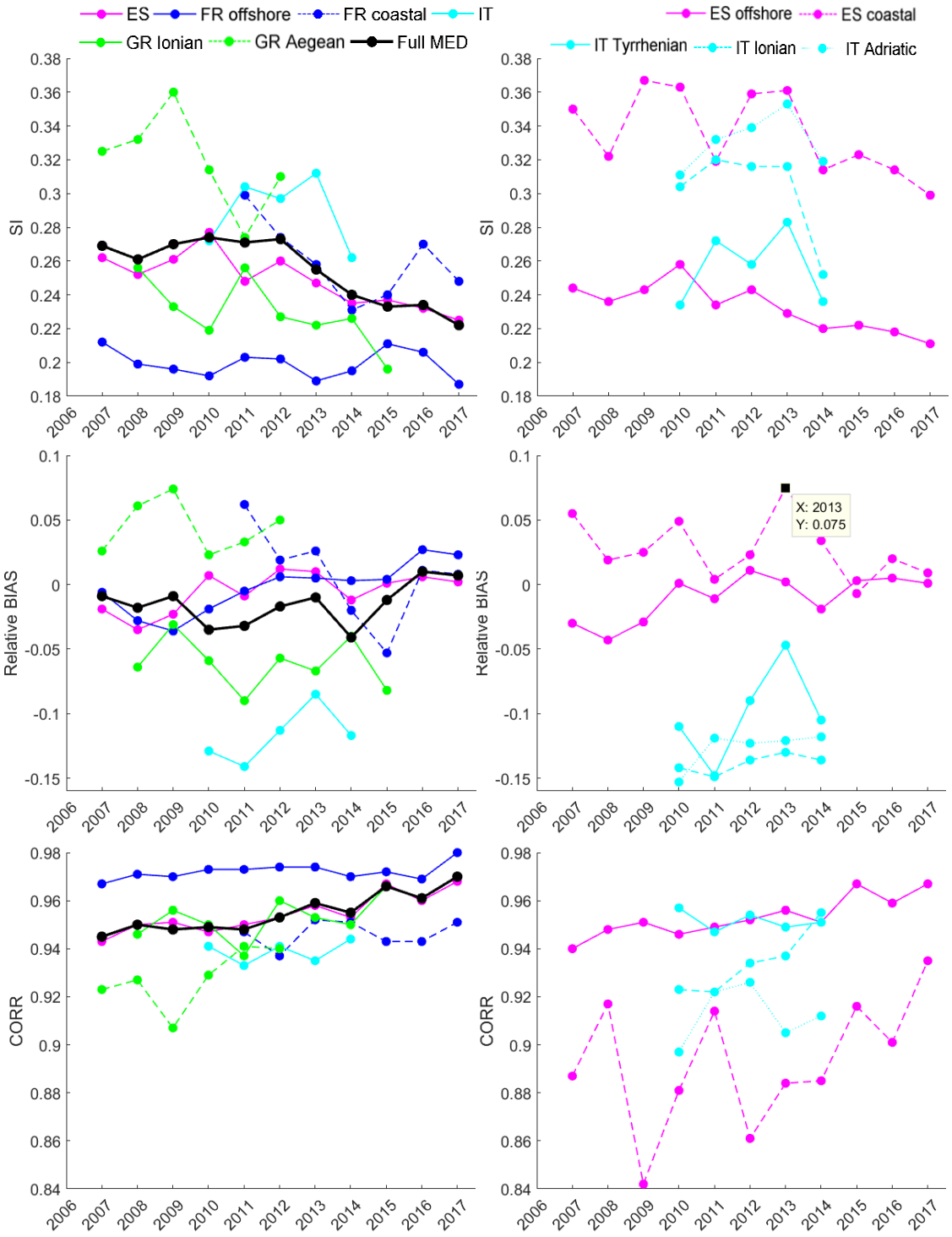

Figure 7: Yearly values of SWH metrics for the full Mediterranean Sea and for the wave buoy groups defined in Table 3. In the legend: ES = Spanish, FR = French, IT = Italian, GR = Greek. Relevant metrics from **Erreur ! Source du renvoi introuvable.**: SWH-H-CLASS2-MOOR-<STAT>-YR-MED, SWH-H-CLASS2-MOOR-<STAT>-YR-<MOORINGS GROUP ID>

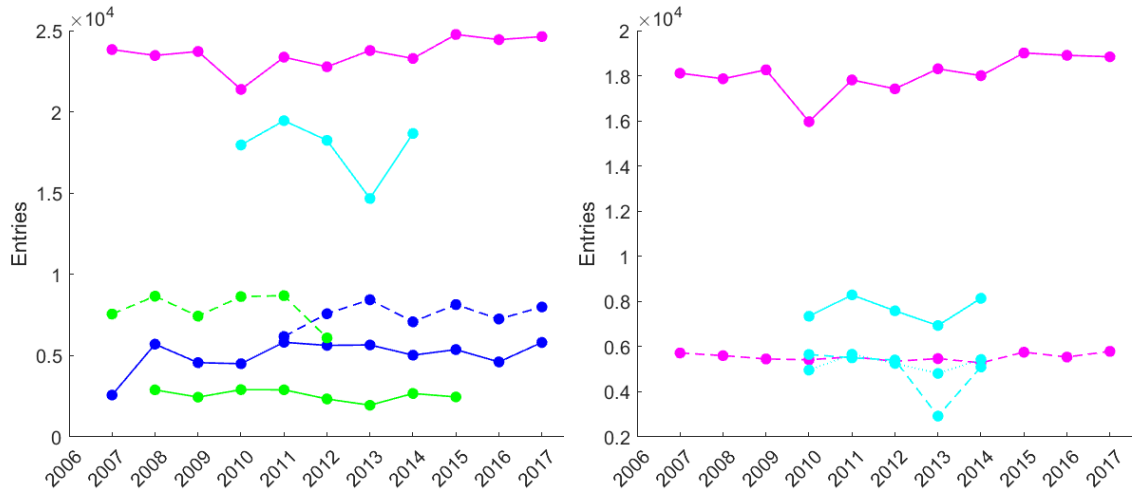

Figure 8: Yearly values of SWH collocations (i.e. entries to the computation of the metrics) for the wave buoy groups defined in Table 3. Legend as in Figure 7.

Figure 7 shows that, for the full Mediterranean Sea, SI values vary from 0.22 to 0.27, relative BIAS from -0.04 to 0.01 and CORR from 0.94 to 0.97. RMSD (not shown) varies from 0.21 m to 0.26 m. The observed variation is very close to the variation obtained for the Spanish wave buoy group, especially for SI and CORR. This is attributed to the fact that model-buoy collocations for this group are the most numerous (Figure 8) over the entire hindcast time span and, as a result, have the greatest impact on the Mediterranean statistics. In general, the yearly size and positioning of the available in-situ observations significantly determine the inter-annual variability of the metrics' values for the full Mediterranean Sea. Consequently, to draw conclusions over the quality evolution of the wave hindcast, one should look at the individual wave buoy groups over long time-scales. In addition, one should examine the quality evolution of the wind forcing. Besides, quality changes should result from specific modifications in the wave and/or the wind modelling systems involved in the hindcast. Modifications that could have impacted the quality of the forcing winds and consequently of the wave hindcast include increases in the wind model horizontal resolution, on January 2010 from 25 km to 16 km and on May 2016 from 16 km to 9 km, and an upgrade in the land-sea mask, orography and climate fields on May 2015. Comparisons between the ECMWF forcing winds and satellite wind observations (see following sub-section) for the period 2007 - 2016 (2017 is missing due to data inadequacy) did not reveal any clear improvement in qualification statistics since 2010. Looking at the individual wave buoy groups in Figure 7, in average, in the period 2010-2012, somewhat better qualification results are seen for the Aegean Sea. Similarly, after 2010, SI and relative BIAS show a small average improvement in the level of 1-2,5% for the Spanish offshore wave buoy group. A similar improvement in relative BIAS is seen for the French offshore buoy group. These quality 'changes' are somewhat more notable than others. The qualification metrics that correspond to the added year of 2017 are amongst the best of the examined period. Regarding the magnitude of the inter-annual variability over the full hindcast period, Figure 7 reveals that the greatest variability in SI (9%) is obtained in the Aegean Sea. Regarding relative BIAS, the greatest variability (11%) is found for the coastal wave group of France. In general, coastal, sheltered and/or surrounded by complex topography wave buoy groups are associated with fair qualification statistics that often show increased inter-annual variability.

Figure 9 shows that SI is consistently higher in summer than in winter with a variation of 0.26-0.32 in the former season and of 0.19-0.25 in the latter. In accordance, CORR (not shown) is consistently lower

in summer (0.92-0.95) than in winter (0.94 - 0.98). On the other hand, with the exception of years 2016-2017, relative BIAS is consistently greater in winter than in summer being mostly negative in the former season whilst frequently changing sign in the latter. Its variation is from -0.04 to 0.01 in winter and from -0.03 to 0.07 in summer reaching the highest value of 0.07 in year 2016 but being otherwise not greater than 0.02.

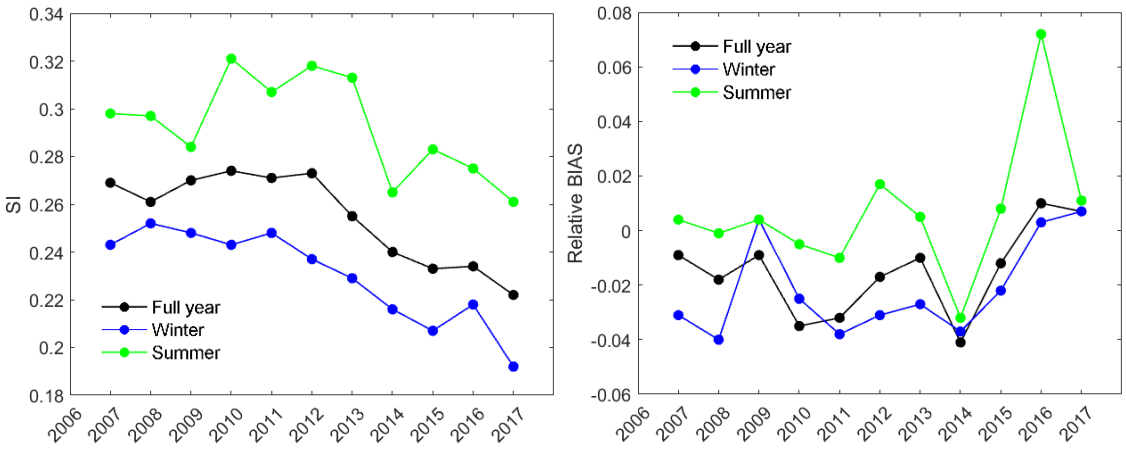

Figure 9: Yearly values of seasonal SWH metrics for the full Mediterranean Sea. Relevant metrics from **Erreur ! Source du renvoi introuvable.**: SWH-H-CLASS2-MOOR-<STAT>-YR-MED.

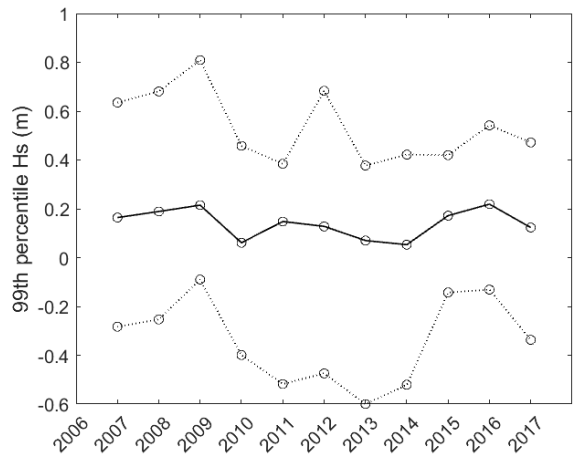

Figure 10: Yearly values of the difference between hindcast and observed 99th percentile of SWH. Solid line: differences computed by merging the wave buoy observations in the Mediterranean Sea. Dashed lines: maximum (upper) and minimum (lower) signed differences found amongst individual wave buoys. Relevant metrics from **Erreur ! Source du renvoi introuvable.**: SWH-H-CLASS2-MOOR-PERC99-YR-MED.

Figure 10 shows that the differences between hindcast and observed 99th percentile of SWH for the full Mediterranean Sea (solid line) vary between 0.06 m and 0.23 m with the largest positive differences found amongst the individual buoy locations (upper dashed line) varying from 0.38 m to 0.81 m and the largest negative differences (bottom dashed line) from -0.61 m to -0.09 m. Overall, throughout the hindcast period, the model mostly overestimates extreme wave heights.

Comparison with satellite observations

This sub-section starts with the comparison of the ECMWF forcing wind speeds, U10, and Med-MFC hindcast SWH with satellite observations of U10 and SWH respectively, separately for each satellite. This is done for the full Q3/2017 hindcast period (2006-2015) and the full Mediterranean Sea. Respective results are shown in Figure 11 (and Tables A2 and A3 in the Appendix).

The most striking features in Figure 11 is a considerable differentiation in model-satellite BIAS found for Ers2 with respects to U10 and for Cryosat2 with respects to SWH. In particular, both U10 model-Ers2 and SWH model-Cryosat2 relative BIAS (BIAS/$\bar{R}$) are found to be different by at least 9% compared to the values computed for the other model-satellite pairs. In addition, BIAS (not shown) is positive for U10 model-Ers2 whilst is negative for all other comparisons for both U10 and SWH. Another observation is that both U10 and SWH model-ers2 SI is about 5% greater compared to the other model-satellite SI values. Otherwise, the model-satellite comparison behaves similarly for the different satellites with the Med-MFC hindcast wave model exhibiting its best performance when compared to the observations of Saral.

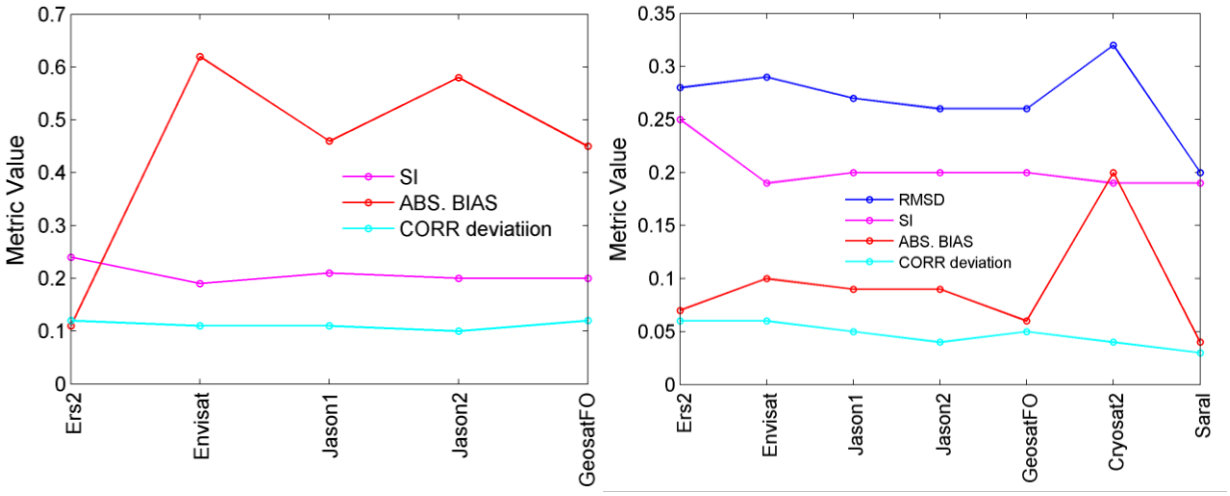

Figure 11: ECMWF analysis U10 (left) and Med-MFC hindcast SWH (right) evaluation against satellite U10 and SWH respectively, for each satellite, for the full Mediterranean Sea, for the full Q3/2017 hindcast period (2006-2015). Relevant metrics from **Erreur ! Source du renvoi introuvable.**: SWH-CLASS4-ALT-<STAT>-10YR-MED for individual altimeters.

It was decided to exclude the observations of Ers2 and Cryosat2 from the analysis done considering merged satellite observations from different satellites. Apart from the aforementioned discrepancies, there are other results obtained in the framework of this study and in the literature to support this decision. Specifically, regarding SWH, satellite-buoy comparisons performed by Sepulveda et al. (2015) have shown that Saral SWH is of better quality than Jason2 and Cryosat2 SWH at both open ocean and coastal buoy sites. In fact, Saral data are of very high quality with no need of corrections whilst corrections are applied to all other satellite SWH observations (corrected data are used herein). After corrections, Jason2 SWH has been found to well approximate Saral SWH whilst less accurate results have been obtained for Cryosat2, particularly for wave heights below 1.5 m (Sepulveda et al., 2015). As a result, in this study, model-Saral SWH metrics' values are considered as the most accurate and satellites leading to considerably different results are excluded from the analysis. Regarding U10, one would expect that model wind and wave scatter distributions against respective observations would

be similar since waves are largely proportional to local generating winds in wind-sea dominated environments as is the Mediterranean Sea. Adopting the scatter plot of hindcast SWH against Saral SWH observations as a benchmark, it was found that, before the performed modification of the default values of the whitecapping dissipation coefficients in WAM (see Section II.2), this was indeed the case for all satellites except for Ers2, i.e. the ECMWF U10 - Ers2 scatter distribution differed substantially from the hindcast SWH - Saral distribution (wind model overestimate over the lower wind speed range accompanied with wave model underestimate over the lower wave height range). Thus, Ers2 observations were excluded from the analysis. The effect of the modification of the whitecapping coefficients is discussed later on in this section.

Table 9 shows statistics from the comparison of hindcast SWH with satellite observations of SWH, for the full Mediterranean Sea, for the full Q3/2017 hindcast period and seasonally (2006-2015). Figure 12 (right) shows the corresponding QQ-Scatter plot for the full hindcast period. Figure 12 (left) shows the equivalent QQ-Scatter plot resulting from the comparison of the ECMWF U10 with satellite measurements of U10.

MED	ENTRIES	$\overline{R}$ (m)	$\overline{M}$ (m)	STD R (m)	STD M (m)	RMSD (m)	SI	BIAS (m)	CORR	LR_SLOPE
Full hindcast	440960	1.25	1.17	0.8	0.83	0.26	0.2	-0.08	0.95	0.95
Winter	86451	1.59	1.51	0.97	1.02	0.30	0.18	-0.08	0.96	0.97
Spring	83917	1.24	1.18	0.76	0.78	0.25	0.20	-0.07	0.95	0.95
Summer	78252	0.93	0.86	0.49	0.49	0.21	0.22	-0.07	0.92	0.93
Autumn	81304	1.19	1.08	0.74	0.77	0.27	0.20	-0.11	0.95	0.93

Table 9: Hindcast SWH evaluation against satellite SWH (Envisat, Jason1, Jason2, GeosatFO, Saral), for the full Mediterranean Sea, for the full Q3/2017 hindcast period and seasonally (2006-2015). Relevant metrics from **Erreur ! Source du renvoi introuvable.**: SWH-CLASS4-ALT-<STAT>-10YR-MED.

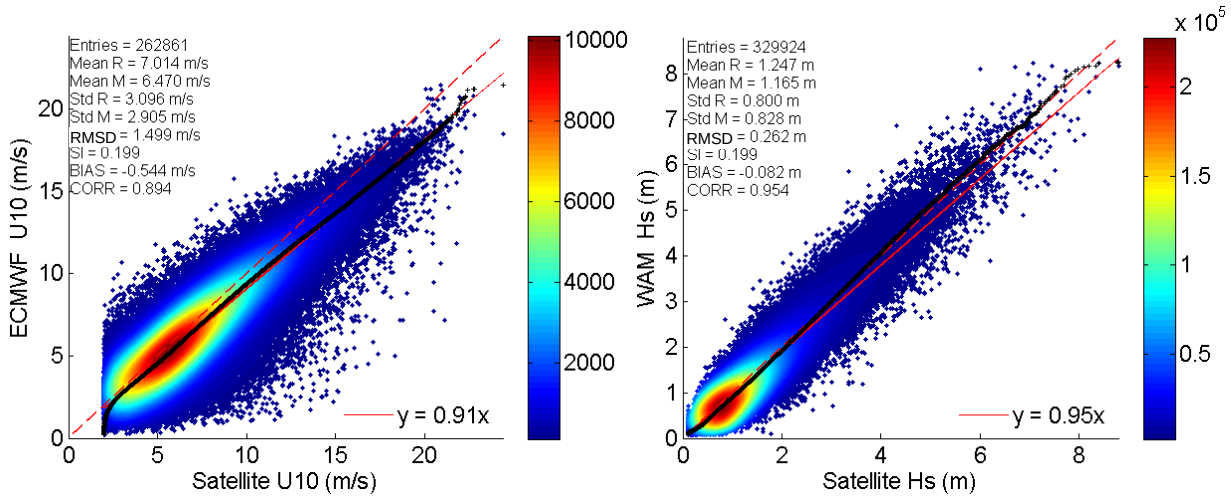

Figure 12: QQ-Scatter plots of: (left) ECMWF U10 versus satellite U10 (Envisat, Jason1, Jason2, GeosatFO); (right) Hindcast SWH (Hs) versus satellite SWH (Envisat, Jason1, Jason2, GeosatFO, Saral), for the full Mediterranean Sea, for the full Q3/2017 hindcast period (2006-2015): QQ-plot (black crosses), 45° reference line (dashed red line), least-squares best fit line (red line). Relevant metrics from **Erreur ! Source du renvoi introuvable.**: SWH-CLASS4-ALT-QQ-10YR-MED, SWH-CLASS4-ALT-SCATTER-10YR-MED.

Figure 12 (left) shows that the ECMWF forcing wind model underestimates observed U10 throughout the entire U10 range, even more so at high wind speeds. An overall model underestimation of about 8% associated with a LR_SLOPE of 0.91 have been computed. Figure 12 (right) also shows an overall wave hindcast underestimation of observed SWH by about 7% associated with a LR_SLOPE of 0.95. Nevertheless, in this case, the model somewhat underestimates observed SWH over the lower SWH range (< 3 m), while, generally, somewhat overestimates larger waves in the data record. This apparent discrepancy between wind and wave scatter distributions is a consequence of the modification of the default values of the whitecapping dissipation coefficients in WAM (see Section II.2). On the whole, Figure 12 shows that the quality of the Med-MFC wave hindcast at offshore locations in the Mediterranean Sea (satellite records near the coast are mostly filtered out as unreliable) is very good. Comparing to the equivalent results obtained from the model-buoy comparison (Figure 4), a smaller scatter (by about 7%) with a larger overall bias (by about 4%) is associated with the model-satellite comparison. The larger BIAS found in this case consists of a greater and more extended underestimate over the lower wave height range and a somewhat smaller overestimate over the higher. SI values compare well at the more exposed wave buoys in the Mediterranean Sea.

Table 9 shows the seasonal variation of the Med-MFC wave hindcast quality. The typical difference (RMSD) varies from 0.21 m in summer to 0.30 m in winter whilst SI is highest in summer (0.22) and lowest in winter (0.18). The SI pattern of variation is similar to the one obtained from the model-buoy comparison despite the lower SI values (by 6-8%) in the current case. Correlation coefficient varies accordingly. In general, as in the model-buoy comparison, a lower scatter with a higher correlation is associated with the more well-defined winter weather conditions. BIAS is negative in all seasons. Relative values (BIAS/$\overline{R}$) are highest in autumn (≈9%) and lowest in winter (≈ 5%). A relative high summer bias of about 7.5% is found in this case which contrasts the 0% bias found in the model-buoy comparison. LR_SLOPE varies from 0.93 in summer and autumn to 0.97 in winter. Overall, Table 9, alike Table 8, reveals that the spring statistics are the most representative of the year-long statistics for the Mediterranean Sea.

Figure 13 maps the statistics of the comparison of ECMWF forcing U10 with satellite observations of U10 (left column) and of Med-MFC hindcast SWH with satellite observations of SWH (right column) for the different sub-regions of the Mediterranean Sea defined in Figure 1. It is noted that the Relative BIAS (BIAS/$\overline{R}$) is displayed in the figure. This quantity allows for a more straightforward comparison between the different sub-basins in terms of percentage deviations from the observed mean value. Tabulated results are presented in Tables A4 (U10) and A5 (SWH) in the Appendix.

Figure 13 (right column) shows that the highest values of SI are found in the North Adriatic (0.27) and Aegean Seas (0.25) whilst the South Adriatic, Alboran, North Tyrrhenian and East Levantine Basin follow (0.22-0.23). SI and CORR have a very similar pattern of variation. In accordance with these results, Ratsimandresey et al. (2008), examining model-satellite agreement over coastal locations of the western Mediterranean Sea, found the worst correlations in the Alboran Sea and east of Corsica Island. Bertotti et al. (2013), in a comparison of high resolution wind and wave model output with satellite data over different sub-regions of the Mediterranean Sea, also found the largest scatter and lowest correlations in the Adriatic and the Aegean Seas. In agreement, Zacharioudaki et al. (2015), focusing on the Greek Seas, have shown a considerably larger scatter in the Aegean Sea than in the surrounding seas, when model output was compared to satellite observations. As explained in the previous sub-section (model-buoy comparison), it is the difficulties of wind models to well-reproduce

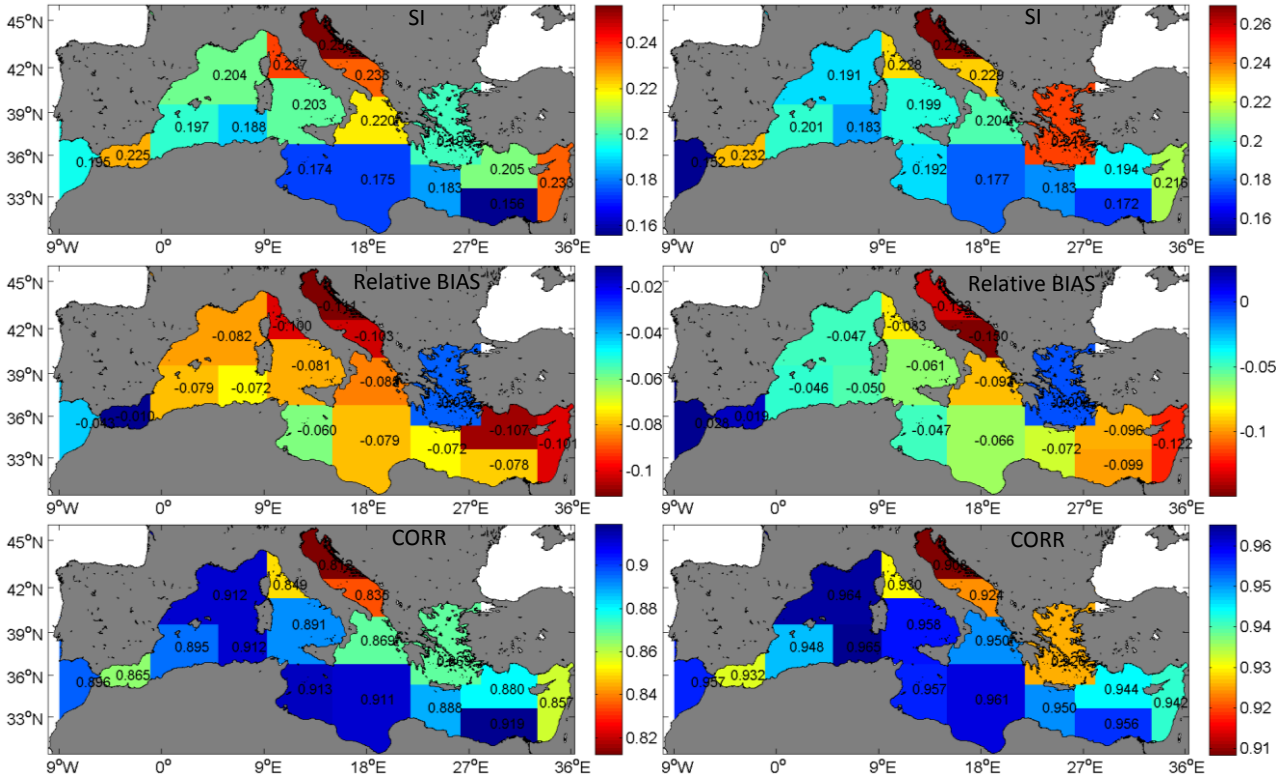

Figure 13: ECMWF U10 (left column) and Med-MFC hindcast SWH (right column) evaluation against satellite U10 (Envisat, Jason1, Jason2, GeosatFO) and satellite SWH (Envisat, Jason1, Jason2, GeosatFO, Saral) respectively: maps of metric values over the Mediterranean Sea sub-regions shown in Figure 1, for the full Q3/2017 hindcast period (2006-2015). Relevant metrics from **Erreur ! Source du renvoi introuvable.**: SWH-CLASS4-ALT-<STAT>-10YR-<REGION>.

orographic effects and/or local sea breezes and the difficulties of wave models to well-resolve complicated bathymetry that introduce errors in these fetch-limited, enclosed regions, often characterized by a complex topography. Indeed, comparison with the equivalent results for the ECMWF wind speeds confirms these difficulties. For example, the pattern of SI and CORR variation for U10 largely resembles that for SWH, corroborating the conclusion of many studies that errors in wave height simulations by sophisticated wave models are mainly caused by errors in the generating wind fields (e.g. Komen et al., 1994; Ardhuin et al., 2007). Nevertheless, some differences do exist. For instance, the SWH SI in the Aegean Sea is relatively higher than the corresponding U10 SI. This is most probably because in this region of highly complicated bathymetry with many little islands the error of the wave model increases in relation to the error of the wind model. Similarly, in the East Levantine, SWH SI is lower than that implied by U10 SI. In this case, the wind model may not well simulate local wind patterns, characterized by local sea breezes and easterly directions (Galil et al., 2006), however, the wave regime which is dominated by waves from the west sector (Galil et al., 2006) is better reproduced by the wave model. Negative BIAS is the case in all sub-regions except for the Atlantic and Alboran Sea. In the latter regions, the wave model overestimates the observations by 2-3%. Otherwise, it underestimates the observations from 1% in the Aegean Sea to about 15% in the Adriatic (adr2). In general, the largest biases are found in the Adriatic, the North Ionian Sea and the Levantine Basin with

values of 9 - 15%. LR_SLOPE (not shown) varies accordingly. QQ-Scatter plots for the individual sub-regions (not shown) have revealed that, in all cases but in the Atlantic, the model underestimates the observations over the lower SWH range but tends to converge or even overestimate the observations as SWH increases. In general, the largest the negative BIAS the more pronounced the underestimate and the smaller the convergence and/or overestimate. In the Atlantic, model overestimate is widespread. Comparing with the equivalent results for the ECMWF wind speed, it is evident that although there are similarities in the pattern of variation of relative BIAS, there are also considerable differences. Notably, in the Alboran Sea and in the Atlantic, a change of sign from negative to positive is observed between wind and waves. As already mentioned, this is a consequence of the modification of the whitecapping dissipation coefficients from default values in WAM, which has led to an important offset of the negative BIAS associated with the ECMWF wind speeds, especially over the high SWH range. Thus, in regions where the ECMWF underestimate has been small, as in the Atlantic, modification of the dissipation coefficients has eventually led to an overshoot of the observed SWH. Figure 13 indicates that the modification of the whitecapping dissipation coefficients has benefited most of the Mediterranean Sea, especially the western part of the basin.

Figure 14-Figure 17 show yearly values of SWH metrics focusing on inter-annual variability. Results shown in these figures are computed considering satellite missions having at least 3 full and continuous years of measurements. Thus, in contrast with the hindcast-long metrics described above, GeosatFO observations (2 full years of data) have being excluded from the analysis whilst Cryosat2 observations have been included.

Figure 14 shows yearly values of SWH metrics for the full Mediterranean Sea computed for individual satellites and for all of them combined. A small inter-annual variability of SI values is evident in the figure which for combined satellite measurements is 0.19-0.21 and for all individual satellites, considered separately, is 0.18-0.21. Relative BIAS for combined satellite measurements varies from -0.11 to -0.05. It is evident that the inclusion of Cryosat2 observations since 2011 has led to an increase of negative bias by up to 5%. Year 2016 constitutes an anomaly of this pattern which is due to an anomalous decrease in the number of Cryosat2 measurements for this year. This dramatic decrease appears to affect the metrics' values computed using Cryosat2 data, leading to the highest negative bias and the poorest correlation computed during the hindcast period, but also leads to the small contribution of Cryosat2 to the combined results. For merged satellite observations, CORR only varies from 0.95 to 0.96 and RMSD (not shown) from 0.23 m to 0.29 m. Equivalent results for ECMWF forcing U10 (not shown) have been found to be in general agreement. No clear jumps or trends in metrics' values have been observed within the hindcast period.

Figure 15 shows the inter-annual seasonal variability of the metrics for the full Mediterranean Sea considering merged satellite observations. Like in the case of model-buoy comparison (Figure 9), Figure 15 shows that SI is consistently higher in summer than in winter. Its variation is 0.2-0.25 in the former season and 0.17-0.2 in the latter. Spring and autumn SI values lie in between. Accordingly, CORR (not shown) is consistently lower in summer than in winter with CORR variation being greater in summer (0.88-0.93) than in winter (0.94-0.97). Spring and autumn CORR values lie closer to winter values. Relative BIAS, contrary to the model-buoy comparison, is consistently greater in summer (-0.14 to -0.07) than in winter (-0.08 to -0.03). Also, the inclusion of Cryosat2 since 2011 seems to affect more summer than winter bias which seems reasonable since Cryosat2 errors, as mentioned above, are mostly associated with low waves (Sepulveda et al., 2015). In accordance with hindcast-long results, the highest negative bias is observed in autumn (-0.14 to -0.08) and this result is largely consistent over the years. Also, spring bias (-0.11 to -0.04), which mostly lies between winter and summer bias, is the closest to full year bias for most of the years examined.

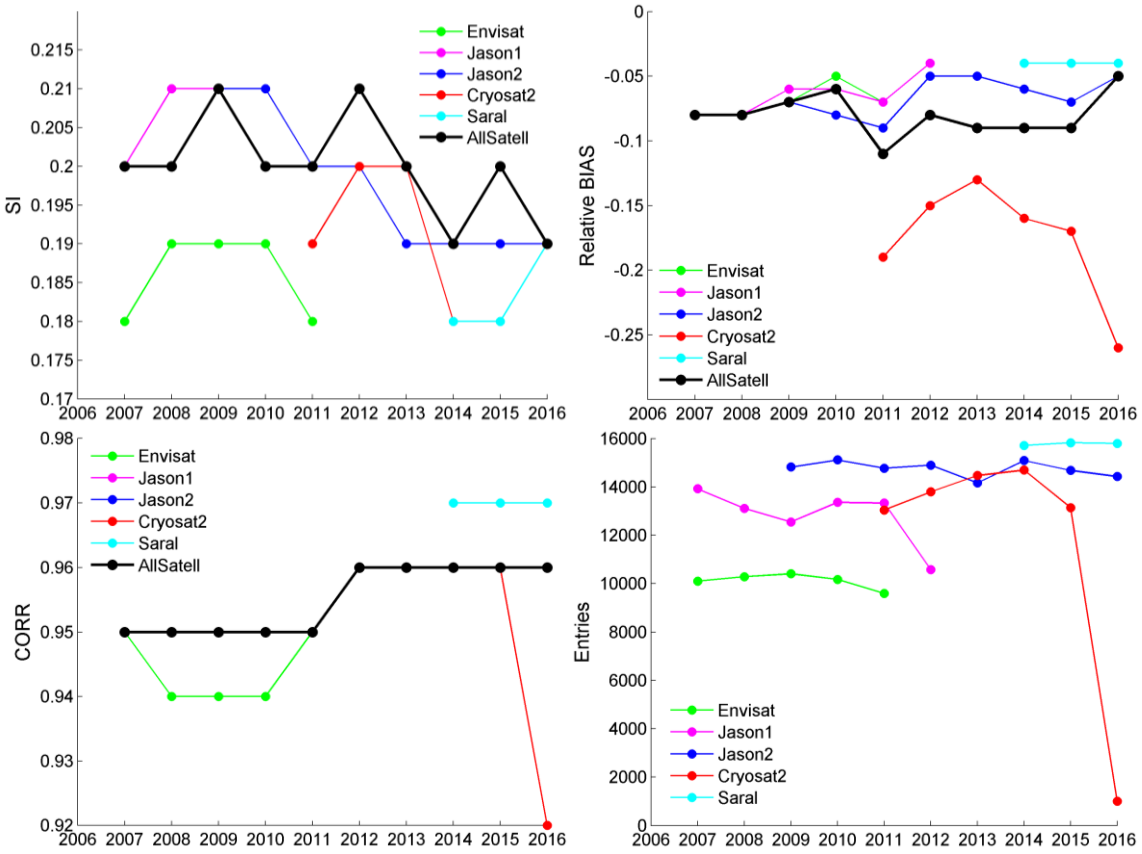

Figure 14: Yearly values of SWH metrics for the full Mediterranean Sea computed for individual satellites and for all of them combined. Relevant metrics from **Erreur ! Source du renvoi introuvable.**: SWH-CLASS4-ALT-<STAT>-YR-MED for merged satellite observations and for individual satellites.

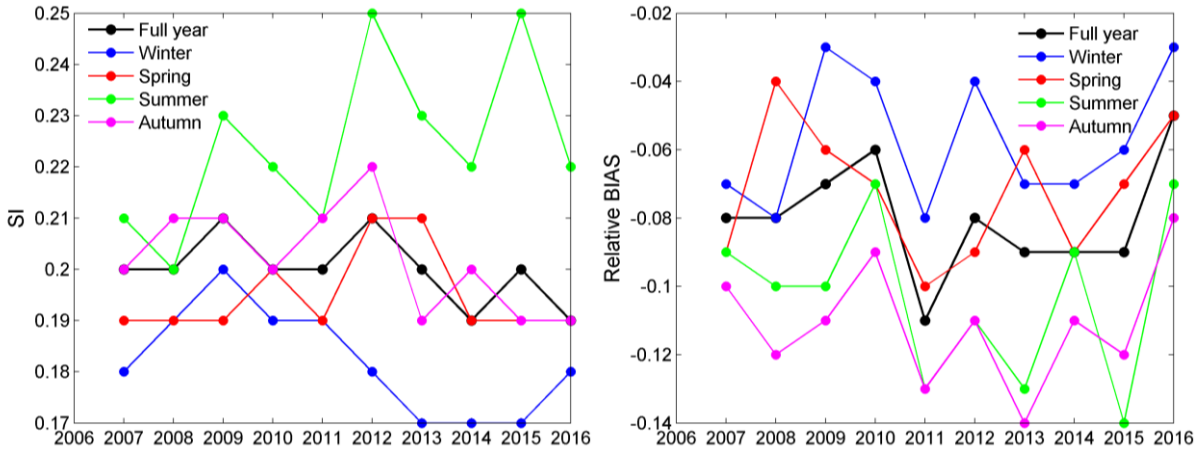

Figure 15: Yearly values of seasonal SWH metrics for the full Mediterranean Sea. Relevant metrics from **Erreur ! Source du renvoi introuvable.**: SWH-CLASS4-ALT-<STAT>-YR-MED.

Figure 16 shows yearly values of the differences between hindcast and observed 99th percentile of SWH for the full Mediterranean Sea when using merged satellite observations (solid line) together with the maximum and minimum signed differences found in the basin when considering equivalent

values for the individual satellites (dashed lines). For merged satellite observations the differences are from 0.01 m to 0.19 m. The maximum signed differences found amongst the individual satellites (upper dashed line) vary from 0.02 m to 0.29 m whilst the minimum signed differences (bottom dashed line) from -0.1 m to 0.09 m. In agreement with the equivalent results obtained from the model-buoy comparison (Figure 10), it is shown that the model tends to overestimate SWH throughout the hindcast period. Nevertheless, in this case, a better and more consistent agreement between modeled and observed extreme wave events is obtained which is manifested by the somewhat lower differences obtained using merged satellite observations but primarily by the much smaller distance between the maximum and minimum differences found amongst the individual satellites.

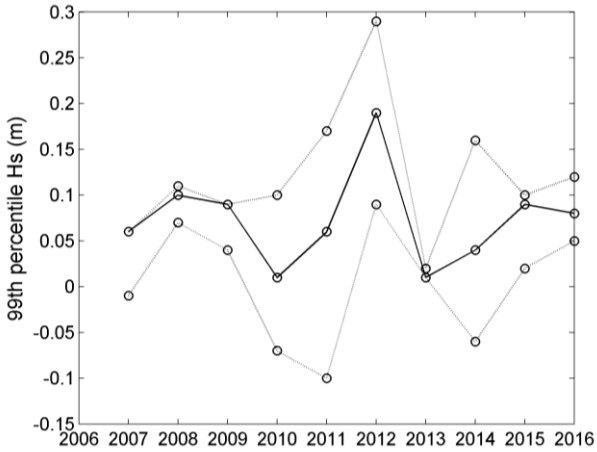

Figure 16: Yearly values of the difference between hindcast and observed 99th percentile of SWH. Solid line: differences computed by merging the satellite observations in the Mediterranean Sea. Dashed lines: largest positive (upper) and largest negative (lower) differences found amongst individual satellites. Relevant metrics from **Erreur ! Source du renvoi introuvable.**: SWH-CLASS4-ALT-PERC99-YR-MED.

Finally, Figure 17 shows the inter-annual variability of SWH metrics for individual sub-regions of the Mediterranean Sea. These sub-regions have resulted from merging those in Figure 1 having the same prefix (the Alboran Sea, alb, is merged with the South West Mediterranean, swm). The yearly relative quality of the wave hindcast output in the different sub-basins is in general agreement with the hindcast-long results depicted in Figure 13. Figure 17 additionally shows that the poorest wave model performance in terms of SI may be found either in the Adriatic or the Aegean Sea depending on the year and that the performance in the southeast Mediterranean Sea (ion and lev) is consistently better than in the west Mediterranean (swm, nwm, tyr). It should be born in mind that although Figure 17 is useful in providing an insight of the possible inter-annual variability of the qualification metrics for the different Mediterranean sub-regions the results depicted may be influenced by the quality of the yearly observations used to perform the model-satellite comparisons (see Figure 11 and Figure 14). This is particularly obvious in relation to relative BIAS where a 'jump' towards increased negative values is observed since the inclusion of Crysat2 observations in 2011 except for year 2016 where a dramatic decrease in Cryosat2 observations has occurred as explained above. This 'jump' appears to be significant for the Adriatic and Aegean Seas, followed by the Tyrrhenian. It looks however not to impact the southeast Mediterranean Sea (ion and lev) where, in general, the most consistent yearly metrics' values are obtained throughout the hindcast period.

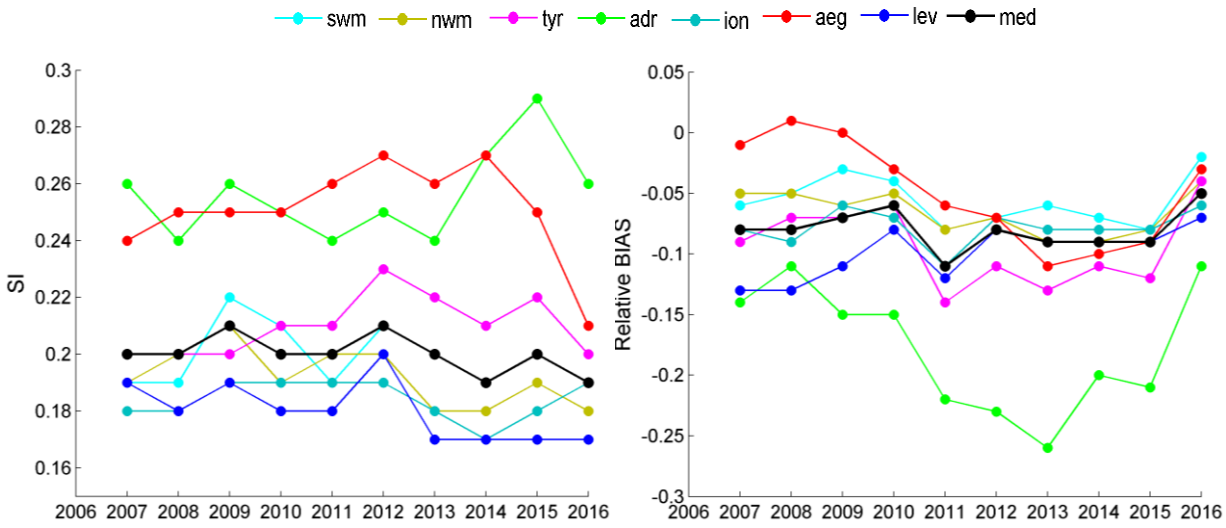

Figure 17: Yearly values of SWH metrics for individual sub-regions of the Mediterranean Sea. Relevant metrics from **Erreur ! Source du renvoi introuvable.**: SWH-CLASS4-ALT-<STAT>-YR-<REGION>.

IV.2 Mean Wave Period

Comparison with in-situ observations

MED	ENTRIES	$\overline{R}$ (s)	$\overline{M}$ (s)	STD R (s)	STD M (s)	RMSD (s)	SI	BIAS (s)	CORR	LR_SLOPE
Whole Year	366410	3.87	3.47	0.91	1.08	0.68	0.14	-0.40	0.86	0.90
Winter	89688	4.15	3.74	1.00	1.20	0.72	0.14	-0.41	0.87	0.91
Spring	91104	3.91	3.51	0.92	1.06	0.67	0.14	-0.40	0.86	0.90
Summer	93663	3.52	3.13	0.68	0.84	0.62	0.14	-0.39	0.82	0.89
Autumn	91955	3.93	3.52	0.92	1.09	0.70	0.14	-0.42	0.86	0.90

Table 10: Hindcast MWP evaluation against wave buoys' SWH, for the full Mediterranean Sea, for the full Q3/2017 hindcast period and seasonally (2006-2015). Relevant metrics from **Erreur ! Source du renvoi introuvable.**: MWP-H-CLASS2-MOOR-<STAT>-10YR-MED.

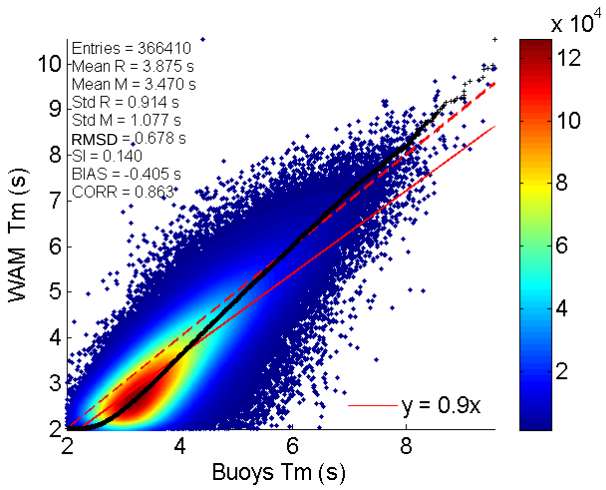

Figure 18: QQ-Scatter plots of hindcast MWP (Hs) versus wave buoys' observations, for the full Mediterranean Sea, for the full Q3/2017 hindcast period (2006-2015): QQ-plot (black crosses), 45° reference line (dashed red line), least-squares best fit line (red line). Relevant metrics from **Erreur ! Source du renvoi introuvable.**: MWP-H-CLASS2-MOOR-QQ-10YR-MED, MWP-H-CLASS2-MOOR-SCATTER-10YR-MED.

Table 10 presents the statistics of the comparison between the hindcast MWP and in-situ observations of MWP, for the full Mediterranean Sea, for the full Q3/2017 hindcast period and seasonally (2006-2015). Figure 18 shows the corresponding QQ-Scatter plot for the full Q3/2017 hindcast period. It is shown that the model exhibits greater variability than the observations (STD in Table 10). RMSD varies from 0.62 s in summer to 0.72 s in winter. The model-observation difference in relation to the mean of the observations (RMSD/$\overline{R}$) is about 17-18%. SI is essentially invariable with a value of 0.14 in all seasons. The non-trivial deviation of SI from relative RMSD (RMSD/$\overline{R}$) indicates that a substantial part of the model-observation difference is caused by BIAS. CORR has its minimum value (0.82) in summer and its maximum (0.87) in winter. As for wave height, the results indicate that the model wave period

follows better the observations in well-defined wave conditions of higher waves and larger periods. BIAS has negative values which correspond to a model underestimate, relative to the observations, of about 10-11%. Correspondingly, LR_SLOPE has a small variation of 0.89-0.91. Figure 18 shows that the wave model underestimates MWP observations below about 6 s while it overestimates larger periods. Measurements of MWP < 4 s are especially underestimated by the model. As for wave height, spring statistics are the most representative of the hindcast-long statistics.

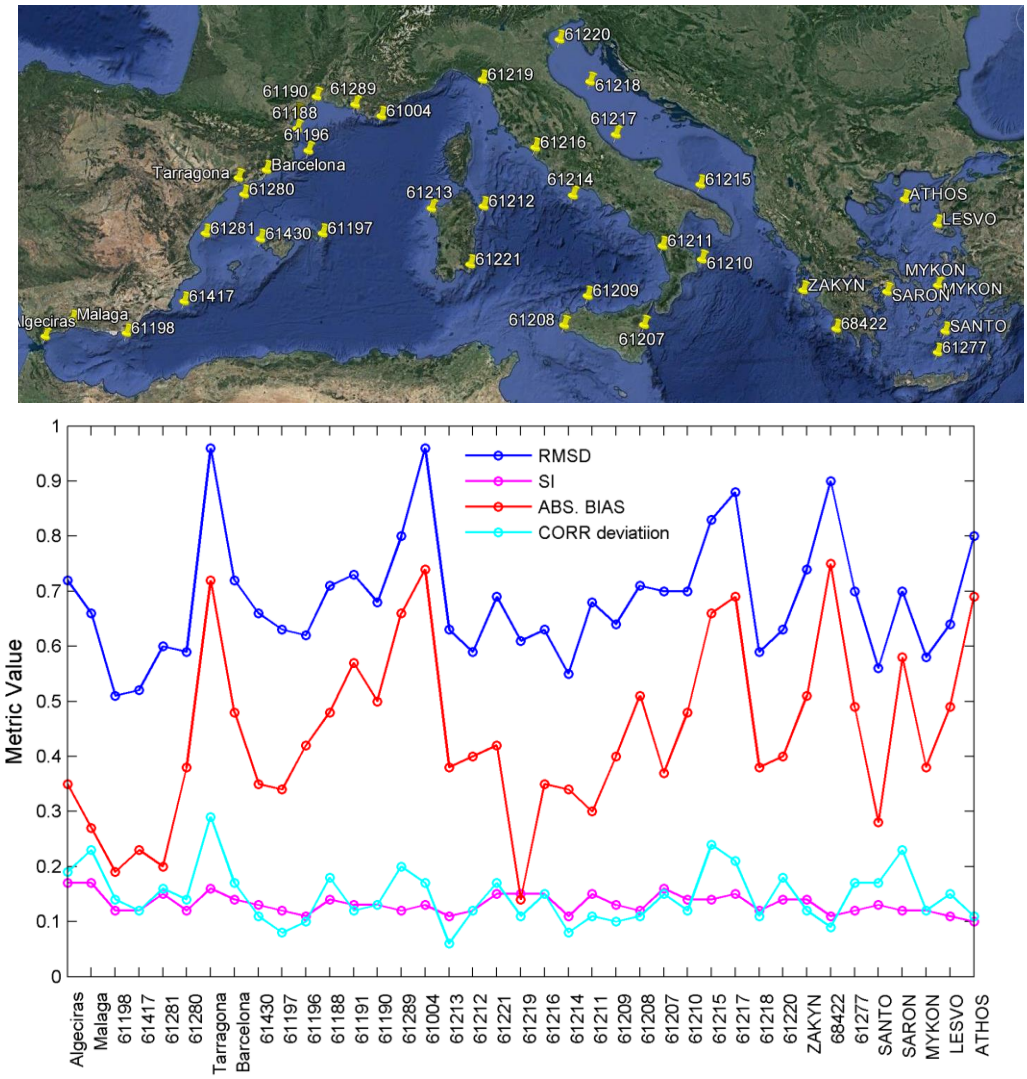

Figure 19: MWP metrics (bottom) at buoy locations (top) for the full Q3/2017 hindcast period (2006-2015). Plot displays metrics starting from the western buoy location and moving eastwards. CORR deviations from unity are shown. Relevant metrics from **Erreur ! Source du renvoi introuvable.**: MWP-H-CLASS2-MOOR-<STAT>-10YR-<MOORING ID>.

Figure 19, like Figure 5, shows the statistics of the model-buoy comparison (bottom panel) at the individual wave buoy locations (top panel). Tabulated results are included in the Appendix (Table A6). As in Figure 5, the absolute BIAS and the CORR deviation from unity are plotted. In this case the original values of BIAS are not included in the figure because BIAS is always negative. The figure shows that the typical model-observation difference, RMSD, varies from 0.51 s (61198) to 0.96 s (Tarragona,

61004). It is evident that this difference is mainly caused by BIAS which is negative at all locations. In relative terms (BIAS/$\overline{R}$), BIAS varies from 4% at buoy location 61219 in the Liguria Sea to 19% at the coastal location of Tarragona. It is only at the former location that the scatter of the data appears to contribute more to the RMSD than the BIAS. In general, model underestimation of the observed MWP appears to be relatively larger over the eastern coast of Spain (Tarragona, Barcelona), all along the French coastline, in the southern Adriatic Sea (61215, 61217) and location 61210, east of southern Italy, as well as at several locations in the Hellenic Seas (notably 68422, SARON and ATHOS). In their majority, these locations are coastal and/or surrounded by complex topography. LR_SLOPE variation (not shown) coincides with the variation of relative BIAS with LR_SLOPE values from 0.81 (Tarragona, 61215, 61217) to 0.98 (61219). QQ-Scatter plots for the individual buoys (not shown) have revealed that the small bias and near unity slope at location 61219 is due to a fairly skewed scatter distribution with non-trivial model underestimation for MWP < 4 s and non-trivial model overestimation for MWP > 4 s. A relatively larger SI is also associated with scatter distributions of a high skewness. In general, a close examination of the QQ-Scatter plots has revealed that the model largely underestimates the observed MWP over the lower wave period range at all locations. Over the higher range, the model overestimates the observed MWP in most of the western Mediterranean Sea west and south of France (except Tarragona). Otherwise, the model mostly underestimates all observed MWP with some convergence towards higher values and, occasionally, some overestimate of the few largest values in the data record. As mentioned above, location 61219 in the Liguria Sea is an exception to this pattern. Also, locations 61211, ZAKYN and SANTO have a distribution more similar to the one obtained for the full Mediterranean Sea (Figure 18). Density scatter plots that appear to have two peaks, although not always very distinct, have also been identified. This is indicative of a double peaked frequency spectrum. Such plots have been obtained for locations (from west to east) Algeciras, 61196, 61213, 61289, 61004, 61208 and MYKON. CORR varies from 0.71 at the coastal location of Tarragona to 0.94 at the well-exposed offshore location 61213 west of Corsica. Generally, in agreement with the wave height results, the lowest correlations are found at coastal locations affected by fetch differences between model and reality due to a complex surrounding topography. On the other hand, the highest correlations are obtained at the most exposed locations in Figure 19 (top). SI is relatively small with values between 0.1 (ATHOS) and 0.17 (Algeciras, Malaga). In the case of MWP, because of the presence of strong biases, SI becomes a less relevant metric in model performance evaluation.

Erreur ! Source du renvoi introuvable. shows yearly values of MWP metrics for the full Mediterranean Sea and for the wave buoy groups defined in Table 3 in Section III. Yearly model-buoy collocation pairs available per wave buoy group are similar to those for SWH shown in Figure 8. **Erreur ! Source du renvoi introuvable.** shows that, for the full Mediterranean Sea, SI values vary from 0.12 to 0.15, relative BIAS from -0.14 to -0.09 and CORR from 0.85 to 0.9. RMSD (not shown) varies from 0.65 s to 0.77 s. Similarly to the equivalent results for the SWH (Figure 7), the observed SI and CORR variations are very close to those obtained for the Spanish wave buoy group. The inter-annual variability of metrics' values exhibited by the Italian wave buoy group is also close to the full Mediterranean variability, especially for relative BIAS. As for SWH, this is because model-buoy collocations for these buoy groups are the most numerous (Figure 8) and, as a result, have the greatest impact on the Mediterranean statistics. As already explained, the yearly size and positioning of the available in-situ observations significantly determines the inter-annual variability of the metrics' values over the full Mediterranean Sea. Looking at the individual wave buoy groups, the greatest inter-annual variability in SI is 3% to 4% and is found for the coastal buoys of Spain, in the Aegean and Adriatic Seas. The same wave buoy groups also exhibit the greatest CORR variability. Regarding relative BIAS, the greatest inter-annual variability of 7% is found for the Spanish wave buoy groups; a non-trivial increase in negative bias is observed for the Spanish wave group in years 2016-2017. In general, the bias found

over the eastern Mediterranean and close to the coast is persistently greater than the bias found offshore the western Mediterranean.

Plots of the inter-annual seasonal variability of metrics' values for the MWP (not shown) have revealed that, in agreement with SWH, CORR is persistently higher in winter (0.85-0.91) than in summer (0.8-0.85). Winter and summer SI values do not differ by more than 1% being mostly greater in winter while respective values of relative BIAS do not differ by more than 3% being mostly greater (in absolute terms) is summer.

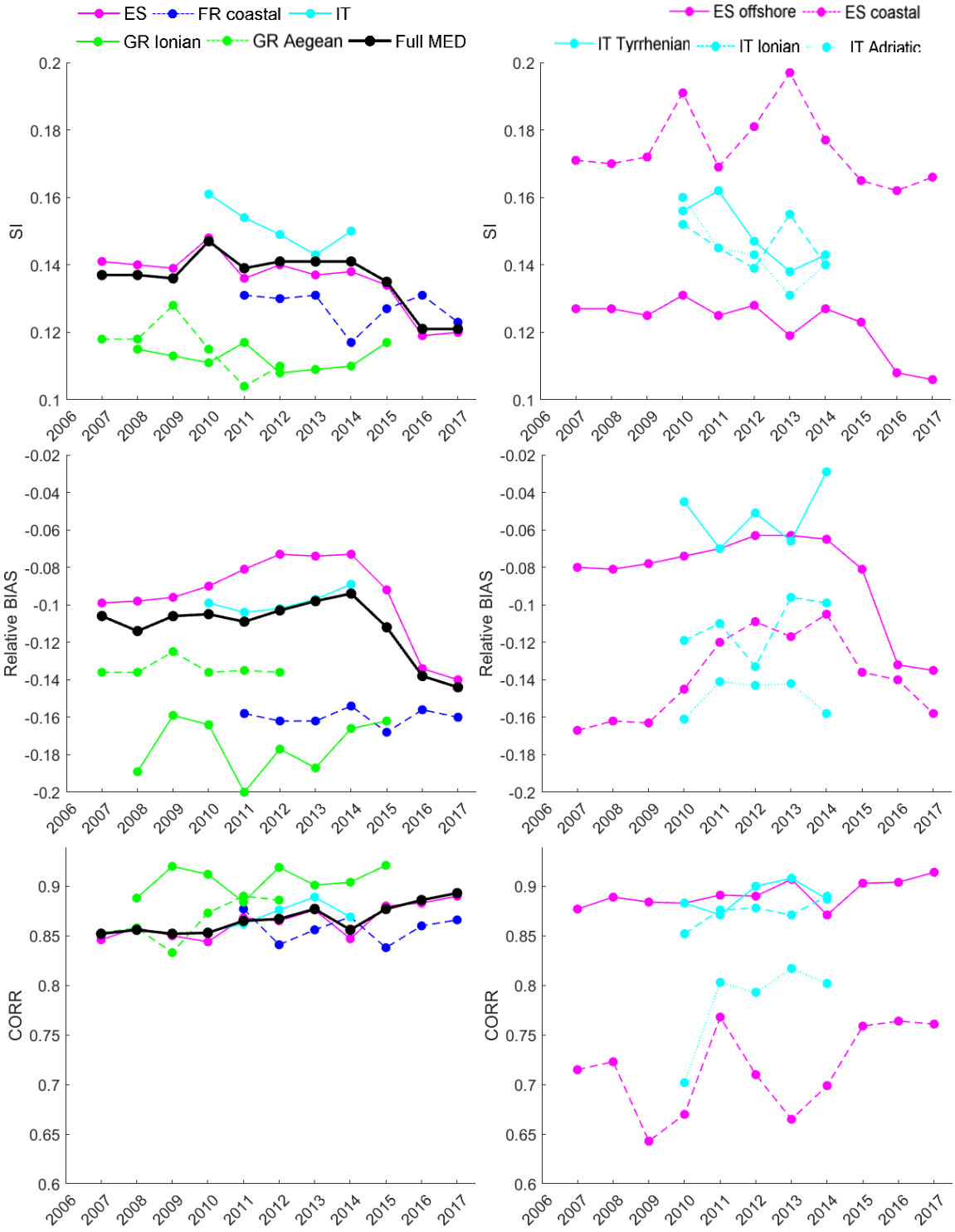

Figure 20: Yearly values of MWP metrics for the full Mediterranean Sea and for the wave buoy groups defined in Table 3. In the legend: ES = Spanish, FR = French, IT = Italian, GR = Greek. Relevant metrics from **Erreur ! Source du renvoi introuvable.**: MWP-H-CLASS2-MOOR-<STAT>-YR-MED, MWP-H-CLASS2-MOOR-<STAT>-YR-<MOORINGS GROUP ID>.

V SYSTEM'S NOTICEABLE EVENTS, OUTAGES OR CHANGES

VI QUALITY CHANGES SINCE PREVIOUS VERSION

Year 2017 has been added to the previous hindcast time series that covered the time period between 2006 and 2016. Validation of the results of year 2017 assured that the quality of the hindcast product remained within expected limits.

VII REFERENCES

Alves, J.-H.G.M., 2006. Numerical modeling of ocean swell contributions to the global wind-wave climate. Ocean Model. 11, 98–122. doi:10.1016/j.ocemod.2004.11.007

Ardhuin, F., Bertotti, L., Bidlot, J.-R., Cavaleri, L., Filipetto, V., Lefevre, J.-M., Wittmann, P., 2007. Comparison of wind and wave measurements and models in the Western Mediterranean Sea. Ocean Eng. 34, 526–541. doi:10.1016/j.oceaneng.2006.02.008

Bertotti, L., Cavaleri, L., Loffredo, L., Torrisi, L., 2013. Nettuno: Analysis of a Wind and Wave Forecast System for the Mediterranean Sea. Mon. Weather Rev. 141, 3130–3141. doi:10.1175/MWR-D-12-00361.1

Bidlot, J.-R., 2015. Intercomparison of operational wave forecasting systems against buoys: data from ECMWF, MetOffice, FNMOC, MSC, NCEP, MeteoFrance, DWD, BoM, SHOM, JMA, KMA, Puerto del Estado, DMI, CNR-AM, METNO, SHN-SM.

Cavaleri, L., Sclavo, M., 2006. The calibration of wind and wave model data in the Mediterranean Sea. Coast. Eng. 53, 613–627. doi:10.1016/j.coastaleng.2005.12.006

Donatini, L., Lupieri, G., Contento, G., Feudale, L., Pedroncini, A., Cusati, L., Crosta, A., 2015. A high resolution wind and wave forecast model chain for the Mediterranean & Adriatic Sea. Towar. Green Mar. Technol. Transp. 859–866. doi:10.1201/b18855-116

ECMWF, 2015. ifs.documentation CY41R1. Part VII: ECMWF Wave - Model documentation 2015 [WWW Document]. URL https://software.ecmwf.int/wiki/display/IFS/CY41R1+Official+IFS+Documentation

Galil, B., Herut, B., Rosen, D.S., Rosentroup, Z., 2006. A Consise Physical, Chemical and Biological Characterizasion of Eastern Mediterranean with Emphasis on the Israeli coast.

GEBCO, 2016. GEBCO 30 arc-second grid [WWW Document]. URL http://www.gebco.net/data_and_products/gridded_bathymetry_data/gebco_30_second_grid/

Gerling, T.W., 1992. Partitioning Sequences and Arrays of Directional Ocean Wave Spectra into Component Wave Systems. J. Atmos. Ocean. Technol. 9, 444–458. doi:10.1175/1520-0426(1992)009<0444:PSAAOD>2.0.CO;2

Günther, H., Behrens, A., 2012. The WAM model. Validation document Version 4.5.4. Intitute of Coastal Research Helmholtz-Zentrum Geesthach (HZG).

Hasselmann, K., 1974. On the spectral dissipation of ocean waves due to white capping. Boundary-Layer Meteorol. 6, 107–127. doi:10.1007/BF00232479

Hasselmann, K., Barnett, T.P., Bouws, E., Carlson, H., Cartwright, D.E., Enke, K., Ewing, J.A., Gienapp, H., Hasselmann, D.., Kruseman, P., Meerburg, A., Müller, P., Olbers, D.J., Richter, K., Sell, W., Walden, H., 1973. Measurements of wind-wave growth and swell decay during the Joint North Sea Wave Project (JONSWAP), Ergänzungsheft 8-12. Deutches Hydrographisches Institut.

Hasselmann, S., Hasselmann, K., 1985. Computations and Parameterizations of the Nonlinear Energy Transfer in a Gravity-Wave Spectrum. Part I: A New Method for Efficient Computations of the Exact Nonlinear Transfer Integral. J. Phys. Oceanogr. 15, 1369–1977.

Hasselmann, S., Hasselmann, K., Allender, J., Barnett, T., 1985. Computations and Parameterizations of the Nonlinear Energy Transfer in a Gravity-Wave Specturm. Part II: Parameterizations of the Nonlinear Energy Transfer for Application in Wave Models. J. Phys. Oceanogr. 15, 1378–1391.

Janssen, P., 1989. Wave-Induced Stress and the Drag of Air Flow over Sea Waves. J. Phys. Oceanogr. 19, 745–754.

Janssen, P., 1991. Quasi-linear Theory of Wind-Wave Generation Applied to Wave Forecasting. J. Phys. Oceanogr. 21, 1631–1642.

Komen, G.J., Cavaleri, L., Donelan, M., Hasselmann, K., Hasselmann, S., Janssen, P., 1994. Dynamics and modelling of ocean waves. Cambridge University Press.

Martínez-Asensio, A., Marcos, M., Jordà, G., Gomis, D., 2013. Calibration of a new wind-wave hindcast in the Western Mediterranean. J. Mar. Syst. 121–122, 1–10. doi:10.1016/j.jmarsys.2013.04.006

NGDC, 2006. 2-minute Gridded Global Relief Data (ETOPO2v2) [WWW Document]. Natl. Ocean. Atmos. Admin., U. S. Dept. Commer. URL http://www.ngdc.noaa.gov/mgg/fliers/06mgg01.html

Queffeulou, P., Croizé-Fillon, D., 2017. Glogal altimeter SWH data set - February 2017. Technical Report. URL ftp://ftp.ifremer.fr/ifremer/cersat/products/swath/altimeters/waves/documentation/.

Ratsimandresey, a. W., Sotillo, M.G., Carretero Albiach, J.C., Álvarez Fanjul, E., Hajji, H., 2008. A 44-year high-resolution ocean and atmospheric hindcast for the Mediterranean Basin developed within the HIPOCAS Project. Coast. Eng. 55, 827–842. doi:10.1016/j.coastaleng.2008.02.025

Semedo, A., Sušelj, K., Rutgersson, A., Sterl, A., 2011. A Global View on the Wind Sea and Swell Climate and Variability from ERA-40. J. Clim. 24, 1461–1479. doi:10.1175/2010JCLI3718.1

Sepulveda, H.H., Queffeulou, P., Ardhuin, F., 2015. Assessment of SARAL/AltiKa Wave Height Measurements Relative to Buoy, Jason-2, and Cryosat-2 Data. Mar. Geod. 38, 449–465. doi:10.1080/01490419.2014.1000470

Snyder, R.L., Dobson, F.W., Elliott, J.A., Long, R.B., 1981. Array measurements of atmospheric pressure fluctuations above surface gravity waves. J. Fluid Mech. 102, 1–59. doi:10.1017/S0022112081002528

WAMDI Group, 1988. The WAM Model—A Third Generation Ocean Wave Prediction Model. J. Phys. Oceanogr. 18, 1775–1810. doi:10.1175/1520-0485(1988)018<1775:TWMTGO>2.0.CO;2

Young, I.R., 1999. Seasonal variability of the global ocean wind and wave climate. Int. J. Climatol. 19, 931–950. doi:10.1002/(SICI)1097-0088(199907)19:9<931::AID-JOC412>3.0.CO;2-O

Zacharioudaki, A., Korres, G., Perivoliotis, L., 2015. Wave climate of the Hellenic Seas obtained from a wave hindcast for the period 1960 – 2001. Ocean Dyn. 65, 795–816. doi:10.1007/s10236-015-0840-z

VIII APPENDIX

Buoy ID	ENTRIES	$\bar{R}$ (m)	$\bar{M}$ (m)	STD R (m)	STD M (m)	RMSD (m)	SI	BIAS (m)	CORR	LR_SLOPE
Algeciras	12282	0.59	0.65	0.44	0.54	0.22	0.36	0.05	0.93	1.1
Malaga	26903	0.45	0.48	0.37	0.4	0.17	0.38	0.04	0.91	1.04
61198	23006	1.02	1.07	0.71	0.76	0.25	0.24	0.05	0.95	1.04
61417	25551	1.02	0.97	0.61	0.62	0.22	0.21	-0.05	0.94	0.95
61281	24904	0.82	0.75	0.5	0.5	0.22	0.25	-0.06	0.91	0.92
61280	26834	0.87	0.83	0.57	0.59	0.21	0.24	-0.04	0.94	0.96
Tarragona	27869	0.51	0.5	0.3	0.31	0.16	0.31	-0.01	0.87	0.96
Barcelona	22371	0.73	0.62	0.45	0.4	0.21	0.25	-0.11	0.92	0.84
61430	23690	1.06	1	0.78	0.76	0.26	0.24	-0.06	0.95	0.93
61197	25578	1.29	1.29	0.98	1	0.27	0.21	0	0.96	1
61196	24328	1.28	1.35	1	1.08	0.32	0.25	0.07	0.96	1.05
61188	16544	0.68	0.66	0.53	0.51	0.2	0.3	-0.02	0.92	0.94
61191	15146	0.67	0.68	0.55	0.51	0.18	0.27	0.01	0.94	0.96
61190	16636	0.61	0.66	0.53	0.54	0.19	0.3	0.05	0.94	1.03
61289	11299	0.9	0.85	0.61	0.59	0.2	0.22	-0.05	0.95	0.94
61004	13744	1.11	1.13	0.75	0.85	0.4	0.36	0.01	0.88	1.01
61002	23736	1.57	1.56	1.16	1.24	0.28	0.18	-0.01	0.97	1.01
61001	21138	1	0.99	0.67	0.77	0.23	0.23	-0.01	0.96	1.02
61213	13547	1.28	1.17	1.12	1.05	0.28	0.2	-0.11	0.98	0.91
61212	4057	0.75	0.67	0.53	0.51	0.21	0.26	-0.08	0.93	0.89
61221	12029	0.68	0.71	0.44	0.52	0.2	0.3	0.03	0.92	1.06
61219	14467	0.81	0.71	0.63	0.6	0.22	0.24	-0.1	0.95	0.89
61216	14520	0.68	0.64	0.52	0.53	0.19	0.27	-0.04	0.94	0.95
61214	13866	0.94	0.87	0.73	0.72	0.23	0.23	-0.07	0.96	0.93
61211	18062	0.73	0.64	0.69	0.65	0.21	0.26	-0.09	0.96	0.89
61209	14913	0.83	0.8	0.7	0.73	0.21	0.25	-0.03	0.96	0.98
61208	13890	1.01	0.95	0.73	0.74	0.21	0.2	-0.06	0.96	0.95
61207	12187	0.64	0.51	0.52	0.45	0.23	0.31	-0.12	0.93	0.81
61210	16130	0.73	0.67	0.62	0.61	0.23	0.3	-0.06	0.93	0.92
61215	16617	0.69	0.56	0.5	0.47	0.23	0.28	-0.12	0.93	0.84
61217	6363	0.62	0.5	0.52	0.45	0.24	0.33	-0.12	0.92	0.8
61218	12099	0.81	0.67	0.64	0.58	0.27	0.28	-0.14	0.94	0.83
61220	13214	0.54	0.49	0.49	0.48	0.22	0.4	-0.04	0.9	0.91
ZAKYN	8905	0.88	0.89	0.61	0.72	0.25	0.29	0.01	0.94	1.04
68422	20991	0.95	0.9	0.73	0.7	0.23	0.23	-0.06	0.95	0.93
61277	15523	0.96	0.97	0.65	0.68	0.24	0.25	0.02	0.93	1.01
SANTO	14000	0.88	0.99	0.53	0.65	0.32	0.34	0.12	0.9	1.13
SARON	15956	0.5	0.46	0.3	0.37	0.18	0.36	-0.04	0.88	0.97
MYKON	16709	0.99	1.02	0.72	0.77	0.31	0.31	0.03	0.92	1.01
LESVO	17575	0.79	0.82	0.54	0.63	0.26	0.33	0.03	0.92	1.05

ATHOS	24869	0.83	0.85	0.74	0.79	0.26	0.31	0.02	0.94	1.02

Table A1: Med-MFC hindcast SWH evaluation against wave buoys' SWH, for each individual buoy location, for the full Q3/2017 hindcast period (2006-2015). Relevant metrics from **Erreur ! Source du renvoi introuvable.**: SWH-H-CLASS2-MOOR-<STAT>-10YR-<MOORING ID>.

Satellite ID	ENTRIES	$\overline{R}$ (m)	$\overline{M}$ (m)	STD R (m)	STD M (m)	RMSD (m)	SI	BIAS (m)	CORR	LR_SLOPE
Ers2	34008	5.93	6.04	2.9	2.82	1.42	0.24	0.11	0.88	0.99
Envisat	60968	7.48	6.86	2.97	2.83	1.52	0.19	-0.62	0.89	0.91
Jason1	91332	6.87	6.41	3.09	2.89	1.49	0.21	-0.46	0.89	0.92
Jason2	105048	6.86	6.28	3.15	2.94	1.5	0.2	-0.58	0.9	0.9
GeosatFO	5513	7.14	6.69	2.96	2.83	1.47	0.2	-0.45	0.88	0.92

Table A2: ECMWF analysis U10 evaluation against satellite U10, for each individual satellite, for the full Mediterranean Sea and the full Q3/2017 hindcast period (2006-2015).

Satellite ID	ENTRIES	$\overline{R}$ (m)	$\overline{M}$ (m)	STD R (m)	STD M (m)	RMSD (m)	SI	BIAS (m)	CORR	LR_SLOPE
ers2	36156	1.1	1.04	0.76	0.78	0.28	0.25	-0.07	0.94	0.95
envisat	62113	1.41	1.31	0.78	0.82	0.29	0.19	-0.1	0.94	0.94
jason1	94531	1.25	1.17	0.8	0.83	0.27	0.2	-0.09	0.95	0.95
jason2	110673	1.22	1.13	0.81	0.84	0.26	0.2	-0.09	0.96	0.95
GeosatFO	18447	1.27	1.21	0.77	0.77	0.26	0.2	-0.06	0.95	0.95
Cryosat2	74880	1.25	1.05	0.76	0.83	0.32	0.19	-0.2	0.96	0.89
Saral	44160	1.05	1.01	0.77	0.78	0.2	0.19	-0.04	0.97	0.97

Table A3: Med-MFC hindcast SWH evaluation against satellite SWH, for each individual satellite, for the full Mediterranean Sea and the full Q3/2017 hindcast period (2006-2015). Relevant metrics from **Erreur ! Source du renvoi introuvable.**: SWH-CLASS4-ALT-<STAT>-10YR-MED.

Region	ENTRIES	$\bar{R}$ (m)	$\bar{M}$ (m)	STD R (m)	STD M (m)	RMSD (m)	SI	BIAS (m)	CORR	LR_SLOPE
atl	12231	6.35	6.08	2.75	2.66	1.27	0.19	-0.27	0.9	0.94
alb	6176	7.08	7	3.11	3.02	1.59	0.23	-0.07	0.87	0.97
swm1	18398	6.93	6.39	3.04	2.88	1.47	0.2	-0.55	0.89	0.91
swm2	12021	7.14	6.63	3.26	3.07	1.44	0.19	-0.51	0.91	0.92
nwm	30834	7.61	6.98	3.78	3.52	1.67	0.2	-0.63	0.91	0.9
tyr1	4565	6.82	6.14	3.01	2.87	1.76	0.24	-0.68	0.85	0.89
tyr2	22864	6.94	6.38	3.08	2.92	1.51	0.2	-0.56	0.89	0.91
ion1	17564	6.96	6.54	2.95	2.79	1.28	0.17	-0.42	0.91	0.93
ion2	43203	6.92	6.37	2.93	2.71	1.32	0.17	-0.54	0.91	0.91
ion3	14725	7.12	6.51	3.15	2.89	1.68	0.22	-0.61	0.87	0.9
adr1	6094	6.95	6.18	3	2.76	1.94	0.26	-0.77	0.81	0.87
adr2	5658	6.99	6.27	2.9	2.74	1.78	0.23	-0.72	0.83	0.88
lev1	14810	7.02	6.51	2.78	2.61	1.38	0.18	-0.51	0.89	0.92
lev2	20552	6.86	6.13	2.95	2.76	1.59	0.21	-0.73	0.88	0.88
lev3	16311	6.53	6.03	2.58	2.36	1.14	0.16	-0.51	0.92	0.91
lev4	12885	5.97	5.37	2.7	2.41	1.51	0.23	-0.6	0.86	0.88
aeg	16307	7.77	7.52	3.09	2.92	1.57	0.2	-0.25	0.87	0.95

Table A4: ECMWF analysis U10 evaluation against satellite U10 (Envisat, Jason1, Jason2, GeosatFO), for each individual Mediterranean Sea sub-region shown in Figure 1, for the full Q3/2017 hindcast period (2006-2015).

Region	ENTRIES	$\bar{R}$ (m)	$\bar{M}$ (m)	STD R (m)	STD M (m)	RMSD (m)	SI	BIAS (m)	CORR	LR_SLOPE
atl	15200	1.71	1.76	0.86	0.89	0.26	0.15	0.05	0.96	1.02
alb	7809	1.16	1.19	0.68	0.74	0.27	0.23	0.02	0.93	1.02
swm1	23149	1.26	1.2	0.77	0.79	0.26	0.2	-0.06	0.95	0.96
swm2	15088	1.5	1.43	1.04	1.05	0.29	0.18	-0.07	0.97	0.96
nwm	38444	1.46	1.39	1.04	1.05	0.29	0.19	-0.07	0.96	0.96
tyr1	5714	1.05	0.96	0.61	0.65	0.25	0.23	-0.09	0.93	0.94
tyr2	29096	1.21	1.14	0.77	0.83	0.25	0.2	-0.07	0.96	0.97
ion1	22000	1.2	1.14	0.76	0.79	0.24	0.19	-0.06	0.96	0.97
ion2	53763	1.3	1.22	0.82	0.82	0.25	0.18	-0.09	0.96	0.94
ion3	18627	1.23	1.12	0.79	0.8	0.28	0.2	-0.11	0.95	0.92
adr1	7844	0.95	0.82	0.59	0.61	0.29	0.27	-0.13	0.91	0.89
adr2	7227	1.04	0.89	0.6	0.62	0.29	0.23	-0.16	0.92	0.88
lev1	18380	1.29	1.19	0.71	0.76	0.25	0.18	-0.09	0.95	0.95
lev2	25580	1.2	1.09	0.68	0.71	0.26	0.19	-0.12	0.94	0.92
lev3	20604	1.21	1.09	0.68	0.71	0.24	0.17	-0.12	0.96	0.92
lev4	16048	1.01	0.89	0.63	0.65	0.25	0.22	-0.12	0.94	0.9
aeg	20705	1.12	1.11	0.65	0.73	0.28	0.25	-0.01	0.93	1.01

Table A5: Med-MFC hindcast SWH evaluation against satellite SWH (Envisat, Jason1, Jason2, GeosatFO, Saral), for each individual Mediterranean Sea sub-region shown in Figure 1, for the full Q3/2017 hindcast period (2006-2015). Relevant metrics from **Erreur ! Source du renvoi introuvable.**: SWH-CLASS4-ALT-<STAT>-10YR-<REGION>.

Buoy ID	ENTRIES	$\bar{R}$ (m)	$\bar{M}$ (m)	STD R (m)	STD M (m)	RMSD (m)	SI	BIAS (m)	CORR	LR_SLOPE
Algeciras	9479	3.66	3.31	0.84	1.06	0.72	0.17	-0.35	0.81	0.91
Malaga	23608	3.52	3.25	0.76	0.93	0.66	0.17	-0.27	0.77	0.92
61198	22700	3.88	3.69	0.78	0.93	0.51	0.12	-0.19	0.86	0.95
61417	25278	3.97	3.74	0.76	0.95	0.52	0.12	-0.23	0.88	0.95
61281	24521	3.64	3.44	0.73	1.02	0.6	0.15	-0.2	0.84	0.96
61280	26361	3.78	3.4	0.74	0.89	0.59	0.12	-0.38	0.86	0.91
Tarragona	26506	3.87	3.15	0.82	0.85	0.96	0.16	-0.72	0.71	0.81
Barcelona	21560	3.92	3.44	0.78	0.97	0.72	0.14	-0.48	0.83	0.88
61430	23377	4.2	3.86	0.93	1.21	0.66	0.13	-0.35	0.89	0.93
61197	25314	4.52	4.18	1.1	1.33	0.63	0.12	-0.34	0.92	0.93
61196	24019	4.23	3.81	0.87	1.04	0.62	0.11	-0.42	0.9	0.91
61188	14602	3.67	3.19	0.83	0.88	0.71	0.14	-0.48	0.82	0.87
61191	12112	3.49	2.92	0.87	0.92	0.73	0.13	-0.57	0.88	0.84
61190	13752	3.44	2.94	0.89	0.91	0.68	0.13	-0.5	0.87	0.86
61289	10434	3.82	3.16	0.69	0.74	0.8	0.12	-0.66	0.8	0.83
61004	13254	4.54	3.8	0.93	1.11	0.96	0.13	-0.74	0.83	0.84
61213	12884	4.5	4.12	1.33	1.48	0.63	0.11	-0.38	0.94	0.93
61212	3712	3.56	3.16	0.85	0.9	0.59	0.12	-0.4	0.88	0.89
61221	10753	3.67	3.26	0.88	0.97	0.69	0.15	-0.42	0.83	0.89
61219	13127	3.88	3.74	0.96	1.26	0.61	0.15	-0.14	0.89	0.98
61216	9708	3.58	3.24	0.88	1.01	0.63	0.15	-0.35	0.85	0.91
61214	12919	3.89	3.55	0.95	1.11	0.55	0.11	-0.34	0.92	0.92
61211	15918	4.08	3.78	1.11	1.32	0.68	0.15	-0.3	0.89	0.93
61209	13442	3.98	3.58	0.98	1.13	0.64	0.13	-0.4	0.9	0.91
61208	13129	4.1	3.59	0.96	1.09	0.71	0.12	-0.51	0.89	0.88
61207	10192	3.65	3.28	1.02	1.13	0.7	0.16	-0.37	0.85	0.9
61210	14190	3.69	3.21	0.95	1.04	0.7	0.14	-0.48	0.88	0.88
61215	12565	3.57	2.91	0.72	0.74	0.83	0.14	-0.66	0.76	0.81
61217	4842	3.68	3	0.81	0.86	0.88	0.15	-0.69	0.79	0.81
61218	9799	3.59	3.21	0.91	1	0.59	0.12	-0.38	0.89	0.9
61220	8855	3.37	2.97	0.8	0.8	0.63	0.14	-0.4	0.82	0.88
ZAKYN	8342	4.01	3.5	0.89	1.12	0.74	0.14	-0.51	0.88	0.88
68422	20375	4.31	3.56	0.93	1.14	0.9	0.11	-0.75	0.91	0.84
61277	15254	4.04	3.54	0.72	0.87	0.7	0.12	-0.49	0.83	0.88
SANTO	13699	3.74	3.46	0.69	0.86	0.56	0.13	-0.28	0.83	0.93
SARON	9689	3.28	2.7	0.51	0.62	0.7	0.12	-0.58	0.77	0.83
MYKON	14755	3.78	3.4	0.8	0.91	0.58	0.12	-0.38	0.88	0.9
LESVO	14899	3.68	3.19	0.67	0.81	0.64	0.11	-0.49	0.85	0.87
ATHOS	19766	3.93	3.23	0.81	0.9	0.8	0.1	-0.69	0.89	0.83

Table A6: Med-MFC hindcast MWP evaluation against wave buoys' MWP, for each individual buoy location, for the full Q3/2017 hindcast period (2006-2015). Relevant metrics from **Erreur ! Source du renvoi introuvable.**: MWP-H-CLASS2-MOOR-<STAT>-10YR-<MOORING ID>.